

Sequential Monte Carlo approximations of Wasserstein–Fisher–Rao gradient flows

Francesca Romana Crucinio*¹ and Sahani Pathiraja†²

¹ESOMAS, University of Turin, Italy & Collegio Carlo Alberto, Turin, Italy

²School of Mathematics & Statistics, UNSW Sydney, Australia

Abstract

We consider the problem of sampling from a probability distribution π . It is well known that this can be written as an optimisation problem over the space of probability distribution in which we aim to minimise the Kullback–Leibler divergence from π . We consider several partial differential equations (PDEs) whose solution is a minimiser of the Kullback–Leibler divergence from π and connect them to well-known Monte Carlo algorithms. We focus in particular on PDEs obtained by considering the Wasserstein–Fisher–Rao geometry over the space of probabilities and show that these lead to a natural implementation using importance sampling and sequential Monte Carlo. We propose a novel algorithm to approximate the Wasserstein–Fisher–Rao flow of the Kullback–Leibler divergence and conduct an extensive empirical study to identify when this algorithms outperforms other popular Monte Carlo algorithms.

1 Introduction

Sampling from a target probability distribution whose density is known up to a normalisation constant is a fundamental task in computational statistics and machine learning. A natural way to formulate this task is optimisation of a functional measuring the dissimilarity to the target probability distribution, typically the Kullback–Leibler (KL) divergence.

Following this point of view, one can derive many popular sampling frameworks including variational inference [Blei et al., 2017], algorithms based on the Langevin dynamics [Roberts and Tweedie, 1996, Durmus et al., 2019] and on kernelised Langevin dynamics [Liu and Wang, 2016]. When the space over which the optimisation is carried out is the Wasserstein space, i.e. probability distributions with bounded second moments equipped with the Wasserstein-2 distance [Ambrosio et al., 2008], the resulting gradient descent scheme is referred to as Wasserstein (W) gradient flow. It is well-known that the W gradient flow of the KL can be implemented by a Langevin diffusion [Jordan et al., 1998, Wibisono, 2018] and easily discretised in time, resulting for instance in the Unadjusted Langevin algorithm (ULA; [Roberts and Tweedie, 1996, Durmus et al., 2019]) and in the Metropolis-adjusted Langevin Algorithm (MALA; [Roberts and Tweedie, 1996]) when a Metropolis–Hastings accept reject step is added after each discretisation step. Convergence of the W gradient flow and of the Unadjusted Langevin algorithm is guaranteed when the target distribution is sufficiently smooth and verifies a log-Sobolev assumption [Vempala and Wibisono, 2019]. Alternative discretisations of the KL Wasserstein gradient flow [Salim et al., 2020, Mou et al., 2021] or its gradient flow with respect to similar optimal transport geometries have been considered in the literature to propose alternative algorithms [Liu and Wang, 2016, Garbuno-Inigo et al., 2020], but their convergence also depends strongly on the log-concavity of the target.

A second class of gradient flows which has gained popularity in recent years is that of Fisher–Rao (FR) gradient flows, i.e. gradient descent w.r.t. the Fisher–Rao or Hellinger–Kakutani distance. Contrary to

*francescaromana.crucinio@unito.it F.R.C. gratefully acknowledges the “de Castro” Statistics Initiative at the *Collegio Carlo Alberto* and the *Fondazione Franca e Diego de Castro*.

†s.pathiraja@unsw.edu.au S.P. gratefully acknowledges funding from UNSW Faculty of Science Research Grant and the Eva Mayr Stihl Foundation.

the Wasserstein metric, which leads to a diffusive behaviour, the Fisher–Rao metric leads to birth-death dynamics in which mass is created or removed. FR gradient flows perform natural gradient descent (see, e.g., Nüsken [2024, Appendix D] and Fujiwara and Amari [1995], Hofbauer and Sigmund [1998], Harper [2009a]).

Exponential convergence of the FR gradient flow for KL does not require a log-Sobolev assumption and can be established under a bounded second moment assumption and mild regularity of the ratio between target and initial distribution [Chen et al., 2023, Theorem 4.1 and Eq. (B.6)], and therefore holds for a wider class of targets. The FR gradient flow for KL is intimately tied to tempering or annealing due to its unit time rescaling [Domingo-Enrich and Pooladian, 2023, Chen et al., 2024] and can also be connected to a mirror descent optimisation scheme for KL [Chopin et al., 2024]. While superior in terms of theoretical behaviour, the FR gradient flow does not naturally lead to stable algorithms, in fact, as noted in [Chen et al., 2024], pure FR dynamics cannot change the support of the distribution, so additional steps need to be added to explore the space. These steps can change the dynamics and can become problematic in high dimensions.

One option to address this shortcoming is offered by kernel methods [Nüsken, 2024, Maurais and Marzouk, 2024, Wang and Nüsken, 2024] which naturally introduce a diffusive part into the (unit time) FR dynamics. A second option, and the main focus of this paper, is to combine the W and the FR gradient flows by making use of the Wasserstein–Fisher–Rao metric [Gallouët and Monsaingeon, 2017] leading to the Wasserstein–Fisher–Rao (WFR) gradient flow. The WFR flow combines the diffusive behaviour of the W gradient flow with the FR flow and enjoys more favourable convergence properties, combining the rate of convergence of the W flow with that of the FR flow [Domingo-Enrich and Pooladian, 2023, Lu et al., 2019]; its numerical approximation can considerably speed up the convergence of gradient based methods for multimodal targets [Lu et al., 2019, 2023] and has been successfully employed to learn Gaussian mixtures [Yan et al., 2024]. Despite its favourable convergence properties, the WFR flow of the KL has remained relatively understudied compared to the W and the FR flow. This is likely due to the difficulty of obtaining stable numerical approximations for the WFR flow. To the best of our knowledge, the only numerical approximations of the WFR flow for the reverse KL are given by the birth-death Langevin algorithms developed in [Lu et al., 2019, 2023].

In this paper we review the main gradient flows used for sampling with particular focus on the Wasserstein–Fisher–Rao flow due to its superior convergence properties (Section 2). We propose an algorithm to approximate the WFR flow of the KL divergence which combines the diffusive behaviour of Langevin based algorithms with importance sampling (Section 3) and empirically show its superior performance w.r.t. the birth-death Langevin dynamics of [Lu et al., 2019, 2023]. We further explore the connections between the WFR gradient flow, importance sampling and sequential Monte Carlo samplers (SMC; [Del Moral et al., 2006]) and identify in the latter a general framework to approximate different FR flows. While connections between sequential Bayesian inference and FR flows have been explored in the discrete time and discrete space setting [Del Moral, 1997, Shalizi, 2009, Harper, 2009b, Akyildiz, 2017, Czégel et al., 2022] and more recently in continuous time and continuous space [Pathiraja and Wacker, 2024]; our focus here is on the sampling problem, in which no underlying sequential structure is present. Our aim is to provide a more stable approximation of the WFR than those currently available in the literature and to investigate for which class of targets our approximations of the WFR flow preserve the superior convergence speed established theoretically.

To summarise, the main contributions of this work are

- We propose a stable algorithm to approximate the WFR flow which combines the diffusive behaviour of Langevin samplers and importance sampling (Algorithm 1) and establish its convergence properties (Proposition 3.1 and 3.2). We show that this algorithm is a particular instance of sequential Monte Carlo samplers.
- We provide an optimisation point of view on sequential Monte Carlo samplers, showing that they provide numerical approximations of many FR type gradient flows of the Kullback–Leibler divergence. We thus establish a parallel result to that of Jordan et al. [1998], Wibisono [2018] which shows that algorithms based on the Langevin diffusion can be seen as numerical approximations of the Wasserstein gradient flow (Section 4).

- We empirically show (Section 5) that Algorithm 1 outperforms the current approximations of the WFR flow and is more robust to initialisation than the W and FR flows. We compare our approximation of the WFR flow with other popular Monte Carlo algorithms and identify regimes in which the addition of the FR correction to the W flow is beneficial. We conclude by providing guidelines for choosing the appropriate algorithm for a given target π .

Notation We endow \mathbb{R}^d with the Borel σ -field $\mathcal{B}(\mathbb{R}^d)$ with respect to the Euclidean norm $\|\cdot\|$ where d is clear from context. We denote by $C^1(\mathbb{R}^d)$ the set of continuously differentiable functions, for all $f \in C^1(\mathbb{R}^d)$ we denote the gradient by ∇f . Throughout this manuscript we denote the target by π and assume $\pi = \exp(-V_\pi)$ for some $V_\pi \in C^1(\mathbb{R}^d)$. The initial distribution is denoted by $\mu_0 = \exp(-V_0)$ with $V_0 \in C^1(\mathbb{R}^d)$. We denote by $\mathcal{N}(x; m, \Sigma)$ the density of a multivariate Gaussian with mean m and covariance Σ .

2 Sampling as optimisation and gradient flows

Let us denote the target distribution over \mathbb{R}^d by π . A natural way to recover π is to consider the optimisation problem

$$\min_{\mu \in \mathcal{P}(\mathbb{R}^d)} \text{KL}(\mu|\pi) = \min_{\mu \in \mathcal{P}(\mathbb{R}^d)} \int \log \frac{\mu(x)}{\pi(x)} \mu(x) dx,$$

which can be solved by following the direction of steepest descent of $\text{KL}(\cdot|\pi)$, given by the gradient flow partial differential equation (PDE)

$$\partial_t \mu_t = -\text{grad}_{\mathfrak{m}} \text{KL}(\mu_t|\pi),$$

where $\text{grad}_{\mathfrak{m}} \text{KL}(\mu|\pi)$ denotes the gradient of $\text{KL}(\cdot|\pi)$ w.r.t. metric \mathfrak{m} [Ambrosio et al., 2008, Carrillo et al., 2024]. Depending on the choice of metric \mathfrak{m} , the gradient $\text{grad}_{\mathfrak{m}} \text{KL}(\mu|\pi)$ takes different shapes; we primarily focus on Wasserstein (W), Fisher–Rao (FR) and Wasserstein–Fisher–Rao (WFR) flows of the Kullback–Leibler divergence.

The gradient flow of $\text{KL}(\mu|\pi)$ w.r.t. the geometry induced by the Wasserstein distance is

$$\partial_t \mu_t(x) = \nabla \cdot \left(\mu_t(x) \nabla \log \left(\frac{\mu_t(x)}{\pi(x)} \right) \right) \quad t \in [0, \infty) \quad (2.1)$$

and corresponds to the Fokker–Planck equation of a Langevin diffusion targeting π [Jordan et al., 1998]. Convergence of the W gradient flow has been widely studied [Durmus et al., 2019, Vempala and Wibisono, 2019] and is guaranteed if π satisfies a log-Sobolev inequality (e.g., Chewi et al. [2024]).

The Fisher–Rao (FR) gradient flow of $\text{KL}(\mu|\pi)$ is obtained by considering the Fisher–Rao (also known as Hellinger) metric [Lu et al., 2019]

$$\partial_t \mu_t(x) = \mu_t(x) \left(\log \left(\frac{\pi(x)}{\mu_t(x)} \right) - \mathbb{E}_{\mu_t} \left[\log \left(\frac{\pi}{\mu_t} \right) \right] \right) \quad t \in [0, \infty), \quad (2.2)$$

and is closely tied to mirror descent [Chopin et al., 2024, Domingo-Enrich and Pooladian, 2023] and birth-death [Lu et al., 2019, 2023] dynamics. Fisher–Rao gradient flows are easily rescaled to the unit time interval as shown in Domingo-Enrich and Pooladian [2023] and Lemma A.2 in a slightly more condensed form. The unit time FR flow is intimately tied to geometric interpolations or annealing [Chopin et al., 2024, Domingo-Enrich and Pooladian, 2023] which are at the basis of sequential Monte Carlo (SMC; Del Moral et al. [2006]), annealed importance sampling (AIS; Neal [2001]), parallel tempering [Geyer, 1991] and the homotopy method [Daum and Huang, 2008].

Combining the two geometries one obtains the Wasserstein–Fisher–Rao (WFR) gradient flow Lu et al. [2019, Theorem 3.1]

$$\partial_t \mu_t(x) = \mu_t(x) \left(\log \left(\frac{\pi(x)}{\mu_t(x)} \right) - \mathbb{E}_{\mu_t} \left[\log \left(\frac{\pi}{\mu_t} \right) \right] \right) + \nabla \cdot \left(\mu_t(x) \nabla \log \left(\frac{\mu_t(x)}{\pi(x)} \right) \right) \quad t \in [0, \infty), \quad (2.3)$$

where the addition of the two components is justified because each is π -invariant. As we will see later, from a sampling point of view the W flow diffuses the samples “horizontally” and promotes exploration of the space

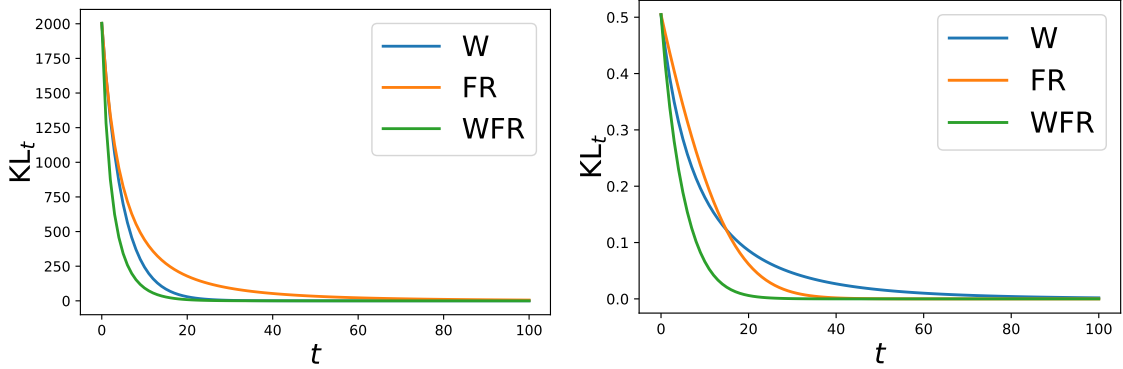


Figure 2.1: Evolution of KL along different PDE flows in the 1D Gaussian case with $\mu_0(x) = \mathcal{N}(x; 0, 1)$ and $\pi(x) = \mathcal{N}(x; 20, 0.1)$ (first row), $\pi(x) = \mathcal{N}(x; 1, 5)$ (second row).

while the FR flows “vertically” weights the samples according to their closeness to the target π . Intuitively, the combination of these two strategies will improve on each one of them.

We briefly review the convergence properties of the WFR flow to showcase its superior theoretical properties compared to the FR and the W flow. The infinite-time FR flow (2.2) reduces $\text{KL}(\mu|\pi)$ w.r.t. the Fisher–Rao distance (e.g., Pathiraja and Wacker [2024, Lemma 2.1]); a similar results holds for the W flow (2.1) w.r.t. the Wasserstein-2 distance under a log-Sobolev assumption on the target π (e.g., [Chewi et al., 2024]):

$$\text{KL}(\mu|\pi) \leq \frac{C_{\text{LSI}}}{2} \int \mu \|\nabla \log \frac{\mu}{\pi}\|^2, \quad (2.4)$$

where C_{LSI} denotes the log-Sobolev constant of π .

To the best of our knowledge, the convergence result obtained under the weakest assumptions on π, μ_0 is given in Chen et al. [2023, Theorem 4.1] and requires that μ_0, π have bounded second moments $\int \|x\|^2 \mu_0(x) dx \leq B$, $\int \|x\|^2 \pi(x) dx \leq B$ and $|\log \mu_0(x)/\pi(x)| \leq M(1 + \|x\|^2)$ for some $M > 0$. Under these assumptions, we have

$$\text{KL}(\mu_t^{\text{FR}}|\pi) \leq M(2 + B + Be)e^{-t},$$

for $t \geq \log((1 + B)M)$. Under (2.4) it is well known that (e.g. Chewi et al. [2024, Section 2.1])

$$\text{KL}(\mu_t^{\text{W}}|\pi) \leq e^{-2C_{\text{LSI}}^{-1}t} \text{KL}(\mu_0|\pi).$$

Due to the orthogonality of the W and FR geometries Gallouët and Monsaingeon [2017, page 13], the convergence rate of WFR gradient flow (2.3) can be upper bounded by Lu et al. [2023, Remark 2.6]

$$\text{KL}(\mu_t^{\text{WFR}}|\pi) \leq \min \{ \text{KL}(\mu_t^{\text{FR}}|\pi), \text{KL}(\mu_t^{\text{W}}|\pi) \}. \quad (2.5)$$

Figure 2.1 shows the evolution of Kullback–Leibler divergence along different PDE flows in the case of 1D Gaussians. The initial distribution is a standard Gaussian and we consider two different targets: for target 1 (first row) we set $m_\pi = 20, C_\pi = 0.1$. In this case the W flow is clearly faster than the FR one and the WFR flow behaves more like the W flow (Figure 2.1 left). For the second target (right) we have $m_\pi = 1, C_\pi = 5$; the FR flow is faster than the W flow for all sufficiently large t , and the WFR flow more closely follows the FR flow. Figure 2.1 confirms that combining the W flow with the FR flow improves on both the W flow and the FR flow.

3 Numerical approximation of the WFR PDE

We now consider numerical approximations of the WFR flow (2.3). Current approximations of the WFR proceed by first discretising space by replacing μ_t with a particle approximation $\mu_t^N = N^{-1} \sum_{i=1}^N \delta_{X_i}$ with

$X_t^i \sim \mu_t$ and secondly discretising time (Lu et al. [2019, 2023] and Lambert et al. [2022, Section H] for Gaussian distributions).

Lu et al. [2019, 2023] consider X_t^i for $i = 1, \dots, N$ which follows a Langevin diffusion to which a birth-death step is added to mimic the FR dynamics (see Appendix E for details). Lambert et al. [2022, Section H] considers weighted particle approximations $\mu_t^N = N^{-1} \sum_{i=1}^N W_t^i \delta_{X_t^i}$ where X_t^i is a Gaussian approximation to μ_t and W_t follows an ODE derived from the FR flow.

We consider a different approach: we first discretise time and then replace μ_n (a time discretised version of μ_t) with a weighted particle approximation $\mu_n^N = N^{-1} \sum_{i=1}^N W_n^i \delta_{X_n^i}$. Considering a time discretisation before a space discretisation allows us to exploit not only the connections between the W flow and Langevin dynamics but also those between the FR flow and mirror descent dynamics [Chopin et al., 2024].

3.1 Time discretisation

The infinite time Wasserstein–Fisher–Rao PDE takes the form

$$\partial_t \mu_t = f_W(\mu_t) + f_{FR}(\mu_t)$$

where $f_W(\mu) := \nabla \cdot (\mu \nabla \log \frac{\mu}{\pi})$ and $f_{FR}(\mu) := \mu (\log \frac{\mu}{\pi} - \int \log \frac{\mu}{\pi} d\mu)$ correspond to the Wasserstein and Fisher–Rao operators respectively, and takes the form of a reaction-diffusion equation.

To obtain a time discretisation of the WFR PDE we consider the solution operator of the W flow and the FR flow separately. Assume that for certain discrete time $n - 1$ the solution of the WFR PDE is given by μ_{n-1} . A discretisation of the W flow for a time step γ leads to

$$\begin{aligned} \mu_{n-1/2}(x) &:= \mathcal{N}(0, 2\gamma \cdot \text{Id}) * [(\text{Id} + \gamma \nabla \log \pi) \# \mu_{n-1}](x) \\ &\propto \int \exp\left(-\frac{1}{4\gamma} \|x - y - \gamma \nabla \log \pi(y)\|^2\right) \mu_{n-1}(y) dy, \end{aligned} \quad (3.1)$$

see, e.g. Wibisono [2018]. The FR flow is not a linear operator, therefore to obtain an explicit expression for its action on $\mu_{n-1/2}$ we consider the solution of the unnormalised FR PDE,

$$\partial_t \rho_t = \rho_t \log \frac{\pi}{\rho_t} \quad (3.2)$$

over time period t , where the above is obtained by applying Lemma A.1 to (2.2). We can evaluate (3.2) directly using the substitution $\nu_t := \log \frac{\rho_t}{\pi}$ which transforms (3.2) into a linear PDE [Chen et al., 2023, Eq. (B.1)],

$$\partial_t \nu_t = \frac{\partial_t \rho_t}{\rho_t} = \log \frac{\pi}{\rho_t} = -\nu_t$$

which has explicit solution $\nu_t = \nu_0 e^{-t} = e^{-t} \log \frac{\rho_0}{\pi}$. Transforming back yields

$$e^{-t} \log \frac{\rho_0}{\pi} = \log \frac{\rho_t}{\pi} \implies \rho_t = \pi^{1-e^{-t}} \cdot \rho_0^{e^{-t}}.$$

Therefore, we immediately obtain that the FR flow with time step γ applied to $\mu_{n-1/2}$ gives

$$\mu_n(x) \propto \pi(x)^{1-e^{-\gamma}} \mu_{n-1/2}(x)^{e^{-\gamma}} = \left(\frac{\pi(x)}{\mu_{n-1/2}(x)}\right)^{1-e^{-\gamma}} \mu_{n-1/2}(x). \quad (3.3)$$

The solution of the FR flow (3.3) corresponds to one step of mirror descent applied to the Kullback–Leibler divergence (see Chopin et al. [2024]).

Alternating between one step of the W solution operator (3.1) and one step of the FR one (3.3) we obtain a discrete-time approximation of WFR PDE. Combining the fact that the mirror descent iterates reduce the Kullback–Leibler divergence as established in Aubin–Frankowski et al. [2022], Chopin et al. [2024] and standard results on the convergence of the unadjusted Langevin algorithm [Vempala and Wibisono, 2019], we can establish that the discrete scheme given by (3.1)–(3.3) converges exponentially fast provided that the step size γ is chosen wisely (see Appendix B for a proof).

Proposition 3.1. *Assume that π satisfies the log-Sobolev inequality (2.4) and that there exists $L_\pi > 0$ such that $\|\nabla V_\pi(x) - \nabla V_\pi(x')\| \leq L_\pi \|x - x'\|$. If $0 \leq \gamma \leq C_{LSI}^{-1}/(4L_\pi^2)$ the approximation of the WFR flow given by (3.1)–(3.3) satisfies*

$$\text{KL}(\mu_n|\pi) < e^{-n\gamma/C_{LSI}}\text{KL}(\mu_0|\pi) + 8\gamma dL_\pi^2 C_{LSI}^{-1}.$$

The first term of the bound in Proposition 3.1 shows that (3.1)–(3.3) reduce the Kullback–Leibler divergence exponentially fast up to an error due to the time discretisation in (3.1). Comparing Proposition 3.1 with Vempala and Wibisono [2019, Theorem 1] we find that, also in discrete time, the rate of WFR is strictly better than that of pure W, in particular the decay of KL induced by the FR flow allows us to obtain a strict inequality.

As in the continuous time case, obtaining a sharp rate of convergence for the WFR flow is challenging. Our proof techniques uses results from the mirror descent literature which only show that the FR part reduces the Kullback–Leibler divergence but do not quantify the reduction in terms of rates, thus the rate in Proposition 3.1 coincides with that of the discrete time W flow in Vempala and Wibisono [2019, Theorem 1] and is not sharp in general.

3.2 A sampling approach to approximate the WFR PDE

The evolution in (3.1) and (3.3) describes one step of the WFR in discrete time; we now show that both the W and the FR flow can be naturally implemented via sampling based ideas.

We consider an initial state for the WFR PDE given by the empirical measure $\mu_0^N = N^{-1} \sum_{i=1}^N \delta_{X_0^i}$ where $X_0^i \sim \mu_0$ for $i = 1, \dots, N$. Given $\mu_{n-1}^N = N^{-1} \sum_{i=1}^N \delta_{X_{n-1}^i}$, an weighted empirical measure approximating μ_{n-1} , we can approximate the W flow in (3.1) exploiting the well-known connections between the W flow and Langevin dynamics [Jordan et al., 1998], a discretisation of (3.1) over timestep γ is given by N copies of the unadjusted Langevin (ULA) scheme

$$X_n^i = X_{n-1}^i + \gamma \nabla \log \pi(X_{n-1}^i) + \sqrt{2\gamma} \xi_n^i, \quad (3.4)$$

where $\xi_n^i \sim \mathcal{N}(0, \text{Id})$ for $i = 1, \dots, N$. The empirical measure $\mu_{n-1/2}^N := N^{-1} \sum_{i=1}^N \delta_{X_n^i}$ provides an approximation to $\mu_{n-1/2}$.

The expression (3.3) shows that given $\mu_{n-1/2}^N$, μ_n can be approximated by importance sampling with unnormalised weights given by $w_n(x) = \left(\frac{\pi(x)}{\mu_{n-1/2}^N(x)} \right)^{1-e^{-\gamma}}$. When the WFR flow is discretised by first approximating the W flow, then the FR flow, the weights can be computed as

$$\begin{aligned} w_n(x) &= \left(\frac{\pi(x)}{\mu_{n-1/2}^N(x)} \right)^{1-e^{-\gamma}} = \left(\frac{\pi(x)}{\mathcal{N}(0, 2\gamma \cdot \text{Id}) * [(\text{Id} + \gamma \nabla \log \pi) \# \mu_{n-1}^N](x)} \right)^{1-e^{-\gamma}} \\ &= \left(\frac{\pi(x)}{N^{-1} \sum_{i=1}^N \mathcal{N}(x; X_{n-1}^i + \gamma \nabla \log \pi(X_{n-1}^i), 2\gamma \cdot \text{Id})} \right)^{1-e^{-\gamma}}, \end{aligned} \quad (3.5)$$

where we used the definition of pushforward measure and convolution integral to obtain the last expression. This gives the following importance sampling approximation to μ_n : $\mu_n^N := N^{-1} \sum_{i=1}^N \delta_{X_n^i}$ where $W_n^i \propto w_n(X_n^i)$.

Alternating between one step of W flow approximated via (3.4) and one step of FR flow approximated via importance sampling with weights (3.5) we obtain an approximation of WFR PDE through sampling-based procedures (Algorithm 1). To avoid the weight degeneracy normally introduced by repeated importance sampling steps, after each FR step we add a resampling step [Jasra et al., 2011]. We will show in Section 4 that this approximation of the WFR PDE is an instance of a well known class of Monte Carlo algorithms: sequential Monte Carlo samplers.

Similarly to the approximations of mirror descent [Dai et al., 2016, Korba and Portier, 2022, Bianchi et al., 2024] and of birth-death Langevin algorithms [Lu et al., 2019, 2023], the cost of computing the approximate weights is linear in N . However, in our case the mixture approximating the denominator is not obtained

from a kernel density estimator introduced purely for numerical purposes, but can be justified from the point of view of the W flow. We directly compare this approximation of the WFR flow with that provided by the birth-death Langevin dynamics in Section 5.

Algorithm 1 SMC-WFR.

- 1: *Inputs:* learning rate γ , initial proposal μ_0 .
- 2: *Initialize:* sample $\tilde{X}_0^i \sim \mu_0$ and set $W_0^i = 1/N$ for $i = 1, \dots, N$.
- 3: **for** $n = 1, \dots, T$ **do**
- 4: **if** $n > 1$ **then**
- 5: *Resample:* draw $\{\tilde{X}_{n-1}^i\}_{i=1}^N$ independently from $\{X_{n-1}^i, W_{n-1}^i\}_{i=1}^N$ and set $W_n^i = 1/N$ for $i = 1, \dots, N$.
- 6: **end if**
- 7: *W flow:* update $X_n^i = \bar{X}_{n-1}^i + \sqrt{2\gamma}\xi_{n-1/2}^i$, where $\bar{X}_{n-1}^i = \tilde{X}_{n-1}^i + \gamma\nabla \log \pi(\tilde{X}_{n-1}^i)$, $\xi_{n-1/2}^i \sim \mathcal{N}(0, \text{Id})$ for $i = 1, \dots, N$.
- 8: *FR flow:* compute and normalize the weights $W_n^i \propto w_n(X_n^i)$ for $i = 1, \dots, N$, where

$$w_n(x) = \left(\frac{\pi(x)}{N^{-1} \sum_{i=1}^N \mathcal{N}(x; \bar{X}_{n-1}^i, 2\gamma \cdot \text{Id})} \right)^{1-e^{-\gamma}}$$

- 9: **end for**
 - 10: *Output:* $\{X_n^i, W_n^i\}_{i=1}^N$
-

Convergence of the numerical approximations provided by Algorithm 1 follows using similar arguments to those usually employed in the sequential Monte Carlo (SMC) literature (see Section 4 for the connection between Algorithm 1 and these methods). We provide convergence bounds for the approximations of μ_n provided at each step of Algorithm 1. As in standard SMC literature, in the case of the μ -iterates we focus on the approximation error for measurable bounded test functions $\varphi : \mathbb{R}^d \rightarrow \mathbb{R}$ with $\|\varphi\|_\infty := \sup_{x \in \mathbb{R}^d} |\varphi(x)| < \infty$, a set we denote by $\mathcal{B}_b(\mathbb{R}^d)$.

We make a stability assumption on the weights w_n . This assumption corresponds to the assumption used in Lu et al. [2019, Theorem 3.2] to prove decay along the FR flow. To control the error introduced by the approximation of the FR flow we also consider the idealised algorithm in which $\mu_{n-1/2}$ can be computed analytically and the weights are given by

$$v_n(x) = \left(\frac{\pi(x)}{\mu_{n-1/2}(x)} \right)^{1-e^{-\gamma}}. \quad (3.6)$$

To ensure this ideal algorithm is also well-behaved we make similar assumptions on v_n .

Assumption 1. *We assume that the weights v_n, w_n are positive everywhere, $v_n(x_n) > 0, w_n(x_n) > 0$ for every $x_n \in \mathbb{R}^d$, and upper bounded $\|v_n\|_\infty < \infty, \|w_n\|_\infty < \infty$.*

Assumption 1 requires the weights to be bounded above, a standard assumption in the SMC literature. $v_n(x_n) > 0$ ensures that the system does not become extinct (i.e. the weights have never all simultaneously taken the value zero). This assumption and some regularity on π allow us to obtain the following finite- N error bound whose proof is provided in Appendix C. We empirically confirm the rate in Proposition 3.2 in Appendix F.1.

Proposition 3.2. *Under Assumption 1, if π is upper and lower bounded, for all $n \geq 0$ and for every $\varphi \in \mathcal{B}_b(\mathbb{R}^d)$,*

$$\mathbb{E} \left[\left| \sum_{i=1}^N W_n^i \varphi(X_n^i) - \int \varphi(x) \mu_n(x) dx \right|^p \right]^{1/p} \leq \frac{\bar{C}_{p,n}(\gamma)}{N^{1/2}}$$

for some finite constant $\bar{C}_{p,n}(\gamma)$.

This result shows that the error accumulated by running Algorithm 1 decays at rate $N^{-1/2}$. We obtain this result under relatively strong assumptions both on π and on φ , which we envisage could be avoided by considering appropriate integrability conditions on both (e.g. [Agapiou et al., 2017]) but would substantially complicate the presentation. For simplicity, in our arguments we only consider multinomial resampling [Gordon et al., 1993] although lower variance resampling schemes exist [Gerber et al., 2019].

The strong law of large numbers can be obtained from the previous result using Markov’s inequality within a Borel-Cantelli argument as shown in e.g. Boustati et al. [2020, Appendix D].

Corollary 3.3. *Under Assumption 1, if π is upper and lower bounded, for all $n \geq 0$ and for every $\varphi \in \mathcal{B}_b(\mathbb{R}^d)$, we have $\mu_n^N(\varphi) \xrightarrow{a.s.} \mu_n(\varphi)$.*

Using standard techniques (e.g. Berti et al. [2006]) given in detail for the context of interest in Schmon et al. [2021, Supplementary Material, Theorem 1], the result of Corollary 3.3 can be strengthened to the convergence of the measures in the weak topology.

Corollary 3.4. *Under Assumption 1, if π is upper and lower bounded, μ_n^N converges almost surely in the weak topology to μ_n , $\mu_n^N \rightharpoonup \mu_n$.*

4 Sequential Monte Carlo as Approximation of WFR Flows

We introduce in this section a class of algorithms known as sequential Monte Carlo samplers [Del Moral et al., 2006] and highlight how different algorithmic choices within this class lead to approximations of the PDE flows described in Section 2, including Algorithm 1.

4.1 Sequential Monte Carlo samplers

Sequential Monte Carlo (SMC) samplers [Del Moral et al., 2006] provide a particle approximation of the sequence of distributions $(\hat{\eta}_n)_{n \geq 0}$ using clouds of N weighted particles $\{X_n^i, W_n^i\}_{i=1}^N$. To build an SMC sampler approximating the sequence $(\hat{\eta}_n)_{n \geq 0}$ one needs a family of Markov kernels $(M_n)_{n \geq 1}$ used to propagate forward the particles, a sequence of backward kernels $(L_{n-1})_{n \geq 1}$ and a resampling scheme.

A resampling scheme is a selection mechanism which given a set of weighted samples $\{X^i, W^i\}_{i=1}^N$ outputs a sequence of equally weighted samples $\{\tilde{X}^i, 1/N\}_{i=1}^N$ in which $\tilde{X}^i = X^j$ for some j for all $i = 1, \dots, N$. For a review of commonly used resampling schemes see [Gerber et al., 2019].

At iteration n the weighted particle set $\{X_{n-1}^i, W_{n-1}^i\}_{i=1}^N$ approximating $\hat{\eta}_{n-1}$ is resampled to obtain the equally weighted particle set $\{\tilde{X}_{n-1}^i, 1/N\}_{i=1}^N$ and the kernel M_n is applied to propose new particle locations $X_n^i \sim M_n(\tilde{X}_{n-1}^i, \cdot)$. At this stage the particle set approximates $\hat{\eta}_{n-1}$, to obtain an approximation of $\hat{\eta}_n$ an importance sampling step is applied with weights proportional to

$$w_n(x_{n-1}, x_n) = \frac{\hat{\eta}_n(x_n)L_{n-1}(x_n, x_{n-1})}{\hat{\eta}_{n-1}(x_{n-1})M_n(x_{n-1}, x_n)}. \quad (4.1)$$

Due to the renormalisation of the weights we do not need the normalising constants of $\hat{\eta}_n, \hat{\eta}_{n-1}$.

The resulting procedure is summarised in Algorithm 2 whose output is a set of weighted samples which approximate $\hat{\eta}_n$. We refer the reader to Chopin and Papaspiliopoulos [2020] for a comprehensive introduction to SMC. Annealed importance sampling can be obtained from Algorithm 2 by omitting the resampling step; however, since it has been empirically [Jasra et al., 2011] and theoretically [Syed et al., 2024] shown that the addition of the resampling step improves the accuracy of the algorithm we do not further consider AIS.

The particle approximations provided by SMC have been widely studied [Del Moral, 2004]. A complete survey of the convergence results available in the literature is beyond the scope of this work, but we highlight that finite- N bounds as Proposition 3.2 are commonly obtained as well as law of large numbers [Crisan and Doucet, 2002], bias estimates [Olsson and Rydén, 2004] and central limit theorems [Chopin, 2004].

Several choices of kernels M_n, L_n are possible. We refer to Del Moral et al. [2006, Section 3.3] for a thorough discussion but mention here some options which will be relevant in the following sections. A

Algorithm 2 SMC samplers [Del Moral et al., 2006].

- 1: *Inputs:* sequences of distributions $(\hat{\eta}_n)_{n \geq 0}$, Markov kernels $(M_n)_{n \geq 1}$, backward kernels $(L_{n-1})_{n \geq 1}$.
 - 2: *Initialize:* sample $\tilde{X}_0^i \sim \hat{\eta}_0$ and set $W_0^i = 1/N$ for $i = 1, \dots, N$.
 - 3: **for** $n = 1, \dots, T$ **do**
 - 4: **if** $n > 1$ **then**
 - 5: *Resample:* draw $\{\tilde{X}_{n-1}^i\}_{i=1}^N$ independently from $\{X_{n-1}^i, W_{n-1}^i\}_{i=1}^N$ and set $W_n^i = 1/N$ for $i = 1, \dots, N$.
 - 6: **end if**
 - 7: *Propose:* draw $X_n^i \sim M_n(\tilde{X}_{n-1}^i, \cdot)$ for $i = 1, \dots, N$.
 - 8: *Reweight:* compute and normalize the weights $W_n^i \propto w_n(\tilde{X}_{n-1}^i, X_n^i)$ in (4.1) for $i = 1, \dots, N$.
 - 9: **end for**
 - 10: *Output:* $\{X_n^i, W_n^i\}_{i=1}^N$
-

popular choice in the literature is to pick M_n to be an MCMC kernel of invariant distribution $\hat{\eta}_n$. In this case, choosing

$$L_{n-1}(x_n, x_{n-1}) = \frac{\hat{\eta}_n(x_{n-1})M_n(x_{n-1}, x_n)}{\hat{\eta}_n(x_n)},$$

i.e. the reversed Markov kernel that is associated with M_n allows to obtain a simplified expression for the weights $w_n(x_{n-1}) = \hat{\eta}_n(x_{n-1})/\hat{\eta}_{n-1}(x_{n-1})$. An alternative to MCMC kernels is given by unadjusted schemes Dai et al. [2022, Section 2.3]. In this case the weights do not simplify, but in some cases the term $L_{n-1}/M_n \approx 1$ and can be ignored (see Section 4.4 for a deeper discussion for the unadjusted Langevin algorithm).

Del Moral et al. [2006, Proposition 1] derives the expression of the optimal backward kernel L_{n-1} which minimises the variance of the weights. This kernel is intractable in most cases; a pragmatic but suboptimal choice is given by the following approximation of the optimal kernel

$$L_{n-1}(x_n, x_{n-1}) = \frac{\hat{\eta}_{n-1}(x_{n-1})M_n(x_{n-1}, x_n)}{\int \hat{\eta}_{n-1}(z)M_n(z, x_n)dz}. \quad (4.2)$$

The resulting weight expression is

$$w_n(x_n) = \frac{\hat{\eta}_n(x_n)}{\int \hat{\eta}_{n-1}(z)M_n(z, x_n)dz}.$$

There is a vast literature on choosing the sequence $(\hat{\eta}_n)_{n \geq 0}$. The following section discusses how different choices lead to numerical approximation of the PDEs described above.

4.2 Wasserstein–Fisher–Rao flow through SMC

Consider the sequence of distributions $(\hat{\eta}_n)_{n \geq 0}$ given by

$$\hat{\eta}_n(x) = \mu_n(x) \propto \pi(x)^{1-e^{-\gamma}} \mu_{n-1}(x)^{e^{-\gamma}} \quad (4.3)$$

where $\gamma = t_n - t_{n-1}$ is a time discretisation step and M_n given by one step of an unadjusted Langevin algorithm targeting π

$$M_n(x_{n-1}, x_n) = \mathcal{N}(x_n; x_{n-1} + \gamma \nabla \log \pi(x_{n-1}), 2\gamma \cdot \text{Id}). \quad (4.4)$$

Using the approximation of the optimal backward kernel (4.2) we obtain the weights

$$w_n(x_n) = \frac{\mu_n(x_n)}{\int \mathcal{N}(x_n; x_{n-1} + \gamma \nabla \log \pi(x_{n-1}), 2\gamma \cdot \text{Id}) \mu_{n-1}(x_{n-1}) dx_{n-1}}. \quad (4.5)$$

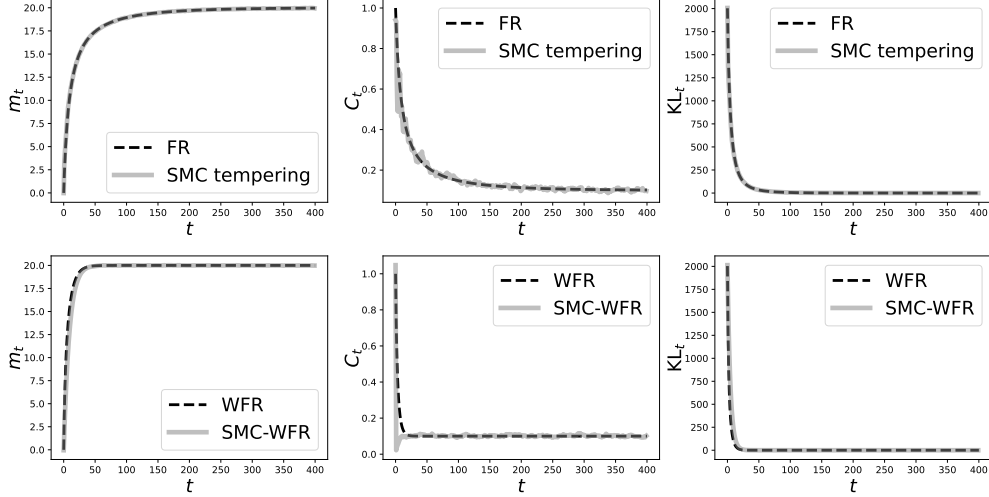


Figure 4.1: Comparison of evolution of mean, variance and KL of the exact PDE flows and approximations provided by Algorithm 2 with target distribution the 1D Gaussian $\pi(x) = \mathcal{N}(x; 20, 0.1)$ and initial distribution $\mu_0(x) = \mathcal{N}(x; 0, 1)$. Top row: Fisher–Rao; bottom row: Wasserstein–Fisher–Rao.

For small γ , we have $\int \mathcal{N}(x_n; x_{n-1} + \gamma \nabla \log \pi(x_{n-1}), 2\gamma \cdot \text{Id}) \mu_{n-1}(x_{n-1}) dx_{n-1} \approx \mu_{n-1}(x_n)$ and we can approximate the weights above with

$$w_n(x_n) = \frac{\mu_{n-1}^{e^{-\gamma}}(x_n) \pi^{1-e^{-\gamma}}(x_n)}{\int \mathcal{N}(x_n; x_{n-1} + \gamma \nabla \log \pi(x_{n-1}), 2\gamma \cdot \text{Id}) \mu_{n-1}(x_{n-1}) dx_{n-1}} \approx \left(\frac{\pi(x_n)}{\int \mathcal{N}(x_n; x_{n-1} + \gamma \nabla \log \pi(x_{n-1}), 2\gamma \cdot \text{Id}) \mu_{n-1}(x_{n-1}) dx_{n-1}} \right)^{1-e^{-\gamma}}.$$

which coincides with (3.5) up to replacing μ_{n-1} with a particle approximation (which will be necessary since μ_{n-1} is unknown also in this case). Different approximations are possible, we choose this one for its similarity with Algorithm 1.

It is now easy to see that the SMC sampler in Algorithm 2 with sequence of distributions (4.3), M_n as the unadjusted Langevin kernel (3.4) and L_{n-1} the approximation of the optimal kernel (4.2) closely resembles Algorithm 1 and provides an approximation of the WFR flow. Figure 4.1 second row compares the approximation provided by Algorithm 1 with the exact evolution of the WFR flow for a 1D Gaussian distribution $\pi(x) = \mathcal{N}(x; 20, 0.1)$.

The main drawback of Algorithm 1 is its higher computational cost. For small number of particles N this additional cost is balanced by the improved convergence speed (Section 5.2) but for large N the $\mathcal{O}(N)$ cost of the weights (3.5) might become prohibitive. In addition (3.5) uses a kernel density estimator-like object to approximate $\mu_{n-1/2}$, which is unlikely to be a good approximation when the dimension is large.

We now discuss some related algorithms which might help circumvent some of these issues.

4.3 SMC tempering

As discussed in Section 3, the solution operator of the infinite time FR flow is given by $\mu_t(x) \propto \pi(x)^{1-e^{-t}} \mu_0(x)^{e^{-t}}$. Consider a time discretisation $0 = t_0, t_1, \dots$ with $t_n - t_{n-1} = \gamma$ and the corresponding discrete time iterates

$$\hat{\eta}_n(x) = \mu_n(x) \propto \pi(x)^{1-e^{-t_n}} \mu_0(x)^{e^{-t_n}} = \mu_{n-1}(x) \left(\frac{\pi(x)}{\mu_0(x)} \right)^{e^{-t_{n-1}} - e^{-t_n}} \quad (4.6)$$

which correspond to the tempering iterates popular in the SMC literature [Chopin et al., 2024].

Consider $\hat{\eta}_n$ to be the n -th tempering iterate (4.6) and as Markov kernel M_n a simple random walk Metropolis (RWM) kernel targeting $\hat{\eta}_n = \mu_n$. Since this choice of M_n leaves $\hat{\eta}_n$ invariant, the weights simplify to

$$w_n(x_{n-1}) = \frac{\hat{\eta}_n(x_{n-1})}{\hat{\eta}_{n-1}(x_{n-1})} = \left(\frac{\pi(x_{n-1})}{\mu_0(x_{n-1})} \right)^{e^{-t_{n-1}} - e^{-t_n}}. \quad (4.7)$$

The resulting SMC algorithm approximates the FR flow as is normally referred to as tempering SMC. Figure 4.1 first row compares the approximation provided by Algorithm 2 and the evolution of the FR flow for a 1D Gaussian distribution $\pi(x) = \mathcal{N}(x; 20, 0.1)$.

As noted in Chen et al. [2024], pure FR dynamics cannot change the support of the distribution, so additional steps need to be added to explore the space. These steps can change the dynamics and can become problematic in high dimensions. The use of a RWM kernel guarantees that the transport dynamics do not alter the sequence of distributions by leaving $\hat{\eta}_n$ invariant.

4.4 Related algorithms: SMC-ULA & SMC-MALA

The main drawback of approximating the WFR flow via Algorithm 1 is the $\mathcal{O}(N)$ cost required to compute the weights (4.5). We consider here two related algorithms that allow to reduce the computational cost of the weight computation.

The first alternative consists in considering a different approximation to (4.5). Since for small γ , we have $\int \mathcal{N}(x_n; x_{n-1} + \gamma \nabla \log \pi(x_{n-1}), 2\gamma \cdot \text{Id}) \mu_{n-1}(x_{n-1}) dx_{n-1} \approx \mu_{n-1}(x_n)$ we can approximate the weights (4.5) with

$$w_n(x_n) = \frac{\mu_{n-1}^{e^{-\gamma}}(x_n) \pi^{1-e^{-\gamma}}(x_n)}{\int \mathcal{N}(x_n; x_{n-1} + \gamma \nabla \log \pi(x_{n-1}), 2\gamma \cdot \text{Id}) \mu_{n-1}(x_{n-1}) dx_{n-1}} \approx \left(\frac{\pi(x_n)}{\mu_{n-1}(x_n)} \right)^{1-e^{-\gamma}}.$$

Using the recursive structure of (4.3) we have

$$\mu_n(x) \propto \pi(x)^{1-e^{-\gamma}} \mu_{n-1}(x)^{e^{-\gamma}} \propto \pi(x)^{1-e^{-2\gamma}} \mu_{n-2}(x)^{e^{-2\gamma}} \cdots \propto \mu_0(x)^{e^{-n\gamma}} \pi(x)^{1-e^{-n\gamma}}$$

and we obtain the simplified weights

$$w_n(x_n) \approx \left(\frac{\pi(x_n)}{\mu_0(x_n)} \right)^{(1-e^{-\gamma})e^{-(n-1)\gamma}}, \quad (4.8)$$

which do not depend on μ_{n-1} but only on π, μ_0 and the time discretisation and can be computed in $\mathcal{O}(1)$ cost w.r.t. N . We call this SMC algorithm SMC-ULA. Our experimental results in Section 5 show that SMC-ULA can be unstable even if SMC-WFR is stable, we believe the use of the different approximations causes this behaviour and is linked to the fact that importance weights obtained from mixture proposals (as (3.5)) have lower variance than those obtained from single proposals (as (4.8)) [Elvira et al., 2019].

A second alternative can be obtained by selecting a different approximation of the W flow. Consider again the sequence (4.3) but now replace the unadjusted Langevin kernel (4.4) with its adjusted version obtained by adding a Metropolis–Hastings accept/reject step, leading to the Metropolis adjusted Langevin algorithm (MALA; Roberts and Tweedie [1996]). We call this SMC algorithm SMC-MALA.

Since MALA leaves π invariant we can select the backward kernel

$$L_{n-1}(x_n, x_{n-1}) = \frac{M_n(x_{n-1}, x_n) \pi(x_{n-1})}{\int M_n(z, x_n) \pi(z) dz} = \frac{M_n(x_{n-1}, x_n) \pi(x_{n-1})}{\pi(x_n)},$$

which leads to the weights

$$w_n(x_{n-1}, x_n) = \frac{\hat{\eta}_n(x_n) \pi(x_{n-1})}{\hat{\eta}_{n-1}(x_{n-1}) \pi(x_n)} = \left(\frac{\mu_{n-1}(x_n)}{\pi(x_n)} \right)^{e^{-\gamma}} \frac{\pi(x_{n-1})}{\mu_{n-1}(x_{n-1})}.$$

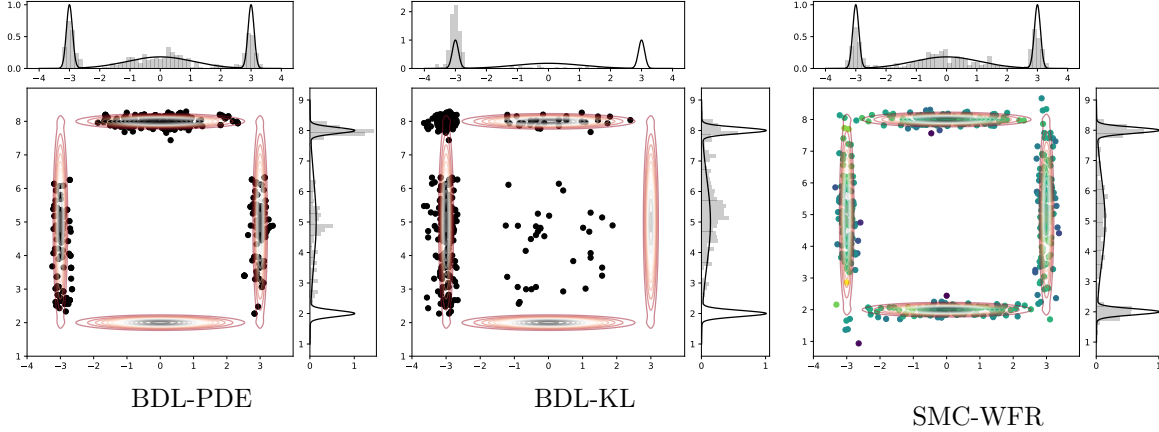


Figure 5.1: Comparison of approximations of the target $\pi(x) = \sum_{i=1}^4 w_i \mathcal{N}(x; m_i, C_i)$ for the birth-death Langevin algorithms and our SMC approximation. For the latter the colour of the particles corresponds to the weight (brighter corresponds to higher weight). We compare both the joint distribution and the marginals.

Using again the recursive structure of (4.3) the above simplifies to

$$w_n(x_{n-1}, x_n) = \frac{\hat{\eta}_n(x_n)\pi(x_{n-1})}{\hat{\eta}_{n-1}(x_{n-1})\pi(x_n)} = \left(\frac{\mu_0(x_n)}{\pi(x_n)} \right)^{e^{-n\gamma}} \left(\frac{\pi(x_{n-1})}{\mu_0(x_{n-1})} \right)^{e^{-(n-1)\gamma}}.$$

The use of a MALA kernel has two advantages over the one described in the previous section: (a) the weights can be computed in $\mathcal{O}(1)$ cost w.r.t. N (against the $\mathcal{O}(N)$ cost of (3.5)) and (b) the discretisation bias introduced by replacing the continuous time Langevin diffusion with its time-discretised approximation (3.4) is removed. While related to SMC-WFR, these algorithms are poor approximations of the WFR flow as shown in Figure F.2 in Appendix F.2.

5 Numerical Experiments

We now present some numerical experiments to support our results in the previous sections. First, we show that SMC-WFR in Algorithm 1 outperforms the birth-death Langevin dynamics as approximation of WFR and show that in a low dimensional setting SMC-WFR converges faster as predicted by the theoretical results in [Lu et al., 2023]. We then compare our SMC approximation of the WFR flow with an approximation the W flow given by N parallel ULA chains and the SMC approximation of the FR flow (i.e. tempering SMC) and compare Algorithm 1 with the variants introduced in Section 4.4. Our aim is to identify scenarios in which the extra computational cost requires by SMC-WFR is beneficial in achieving faster convergence to the target.

Due to the impossibility of accurately approximating KL in general scenarios, to evaluate convergence we consider the maximum mean discrepancy with standard Gaussian kernel (MMD; Gretton et al. [2012]) and the average Wasserstein-1 distance for each 1D marginal (W_1). Code to reproduce our experiments is available at <https://github.com/FrancescaCrucinio/SMC-WFR>.

5.1 Birth-death Langevin and sequential Monte Carlo Wasserstein Fisher Rao

We compare the approximation of the WFR flow (2.3) provided by Algorithm 1 with that given by the birth-death Langevin (BDL) algorithms of Lu et al. [2023, 2019]. We consider the two dimensional Gaussian

Method	MSE mean	MSE covariance	W_1	MMD	runtime (s)	MMD < ϵ
BDL-PDE [Lu et al., 2019]	1.930	4.600	1.325	0.123	3.96	977
BDL-KL [Lu et al., 2023]	2.406	5.645	1.451	0.153	4.87	980
SMC-WFR	0.007	0.043	0.176	0.005	3.79	289

Table 1: Comparison of the approximation of the WFR flow (2.3) provided by the birth-death Langevin (BDL) algorithms and Algorithm 1. We compare the mean squared error MSE for mean and covariance, the average Wasserstein-1 distance over dimension and the maximum mean discrepancy with Gaussian kernel (MMD). We also report the average runtime and the number of iterations needed to have $\text{MMD} < \epsilon$ for $\epsilon = 0.05$. All results are averaged over 50 replicates.

mixture of Lu et al. [2019], given by $\pi(x) = \sum_{i=1}^4 w_i \mathcal{N}(x; m_i, C_i)$ with

$$w_i = 1/4, i = 1, \dots, 4, m_1 = (0, 8)^T, m_2 = (0, 2)^T, m_3 = (-3, 5)^T, m_4 = (3, 5)^T,$$

$$\Sigma_1 = \Sigma_2 = \begin{pmatrix} 1.2 & 0 \\ 0 & 0.01 \end{pmatrix}, \Sigma_3 = \Sigma_4 = \begin{pmatrix} 0.01 & 0 \\ 0 & 2 \end{pmatrix}.$$

The initial distribution μ_0 is a Gaussian with $m_0 = m_1$ and covariance matrix $\Sigma_0 = 0.3 \cdot \text{Id}$. We use $N = 500$, $T = 1000$, $\gamma = 0.01$ and select $h = \gamma$ for the kernel density estimator used within BDL. We compare the results in terms of mean, variance, W_1 and MMD. Both algorithms have $\mathcal{O}(N^2)$ cost due to the computation of the birth-death rates and weights, in fact, they also have the same wallclock time when using the same number of iterations and of particles (Table 1).

The results provided by our SMC approximation are considerably better than those obtained by the BDL algorithms. We attribute this improved performance to three factors. First, the approximations of the birth-death rate (E.1) employed within the BDL algorithms are obtained using kernel density estimation (KDE) while the use of the convolution in (3.5) is motivated by the presence of the W flow and therefore does not add a layer of approximation as does KDE. Secondly, in SMC-WFR the reweighting step corresponds to the exact solution of the FR flow (3.3) in which μ_n is replaced by a particle approximation μ_n^N ; BDL does not use the exact solution but a discretisation of the FR flow obtained through birth-death dynamics. Thirdly, importance (re)sampling seems to be a more algorithmically stable way to approximate the FR flow in the sampling context as it ensures that the number of samples N remains fixed with no additional cost while the BDL dynamics require additional steps to endure that N is kept constant at each time step.

5.2 Robustness to initial distribution

Figure 2.1 suggests that WFR is more robust to the choice of initial distribution: when μ_0 is more concentrated than π , WFR is closer to the FR flow, viceversa, WFR is closer to W when μ_0 is more diffuse than π . We empirically show that this behaviour is maintained by Algorithm 1 when compared with ULA (3.4) (as approximation of the W flow) and the SMC tempering algorithm in Section 4.3 (as approximation of the FR flow).

We fix $\mu_0(x) = \mathcal{N}(x; 0, 1)$ and consider two 1D Gaussian mixture targets

$$\pi_1(x) = \frac{1}{2} \mathcal{N}(x; 0, 1) + \frac{1}{2} \mathcal{N}(x; m, 1), \quad \pi_2(x) = \frac{1}{2} \mathcal{N}(x; 5, 0.1) + \frac{1}{2} \mathcal{N}(x; 6, 0.1).$$

The first target is challenging for the W flow as its log-Sobolev inequality increases exponentially with m [Schlichting, 2019], while the second target is challenging for FR due to the presence of two very peaked modes.

For each algorithm we set $N = 200$ and $\gamma = 0.05$. For ULA we run N parallel chains using the same γ . Figure 5.2 shows the decay of W_1 against iteration number averaged over 50 repetitions for the three algorithms. For π_1 SMC tempering is the fastest than ULA and viceversa for π_2 . SMC-WFR is able to follow the behaviour of the fastest converging algorithm in both cases. However, the cost of SMC-WFR is higher than ULA and SMC tempering. When taking runtime into account, SMC-WFR achieves faster convergence than ULA and is comparable to SMC tempering for π_1 , for π_2 SMC-WFR is faster than SMC tempering and comparable to ULA.

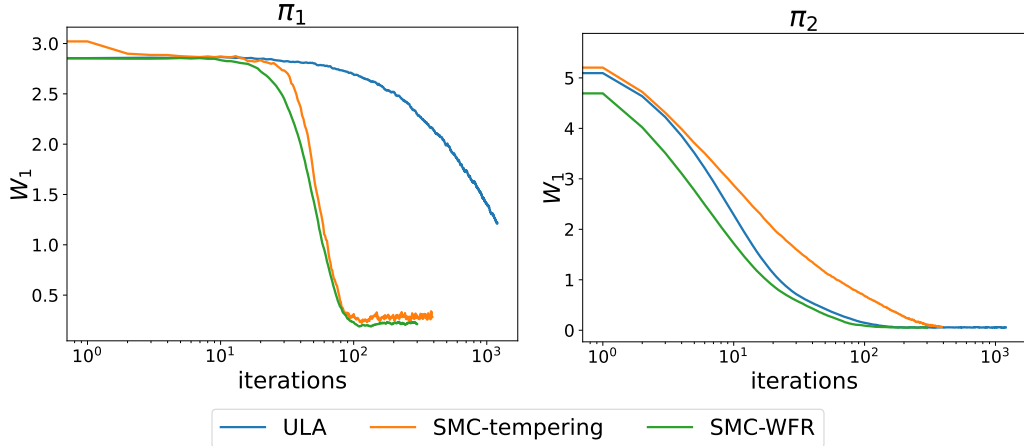


Figure 5.2: 1D Gaussian mixture (Section 5.2): Evolution of W_1 for ULA, SMC tempering and SMC-WFR along iterations averaged over 50 repetitions. The initial distribution is $\mu_0(x) = \mathcal{N}(x; 0, 1)$. Left: π_1 with $m = 6$ is more diffuse than μ_0 . Right: π_2 is more concentrated than μ_0 .

5.3 Comparison with other Monte Carlo algorithms

To assess whether the approximation of WFR in Algorithm 1 preserves the superior convergence speed of the WFR flow we compare SMC-WFR with several sampling algorithms in the literature. In particular we consider N parallel ULA chains (3.4) and N parallel MALA chains [Roberts and Tweedie, 1996] and the SMC tempering algorithm in Section 4.3. We also include SMC-ULA and SMC-MALA (Section 4.4). We consider the following targets (see Appendix F.3 for details): 2D and 20D Gaussian mixture, 2D banana distribution, 2D donut distribution, 20D Gaussian.

We fix $\mu_0(x) = \mathcal{N}(x; \mathbf{0}, \text{Id})$. We tune the variance of the proposal for MALA and SMC-MALA to achieve 57% acceptance rate and the variance of RWM for SMC tempering to achieve 23% acceptance rate [Roberts and Rosenthal, 2001]. For SMC-WFR and SMC-ULA we set γ depending on the target, we use this γ also for the reweighting step in SMC-MALA and SMC tempering (see Appendix F.3 for the experimental setup and additional results).

As the algorithms have different computational cost, we compare them both in terms of number of iterations and in terms of wall-clock time. We summarise our main takeaways as follows:

- (a) **Shape of the target:** When ULA works well, e.g. targets which satisfy a log-Sobolev inequality (2.4) with small C_{LSI} , SMC-WFR and SMC-ULA (both approximating the WFR flow) are competitive in terms of number of iterations to convergence. When ULA works well, convergence tend to be driven by the W flow and SMC-WFR and SMC-ULA perform similarly (Figure F.5, F.6 and F.7). On targets with challenging geometries (Figure 5.3) SMC-WFR achieves faster converge in terms of wallclock time even when ULA, MALA, SMC-ULA and SMC-MALA fail to converge.
- (b) **Computational cost:** SMC-WFR is generally more expensive than the other competitors due to the structure of the weights (3.5), despite this, SMC-WFR tends to converge faster in wallclock time on targets with challenging geometries (Figure 5.3 and 5.4), is competitive on targets where ULA works well (Figure F.5, F.6 and F.7), although ULA and MALA tend to be faster on these targets due to their lower computational cost, and can stabilise the behaviour of ULA in cases where $\nabla \log \pi$ is only locally Lipschitz continuous (Figure F.4).
- (c) **Robustness:** All algorithms are sensitive to step size specification. MALA, SMC-tempering and SMC-MALA are more robust than ULA, SMC-WFR and SMC-ULA but this is largely due to the availability of simple tuning strategies for the proposal variance. SMC-WFR is more robust to the choice of initial distribution, performing well when the initial distribution is more diffuse than the target and when is more concentrated (Figure 5.3 and 5.4).

- (d) **Time discretisation bias:** Due to the lack of the Metropolis–Hastings accept/reject step, ULA, SMC-ULA and SMC-WFR exhibit a time discretisation bias.

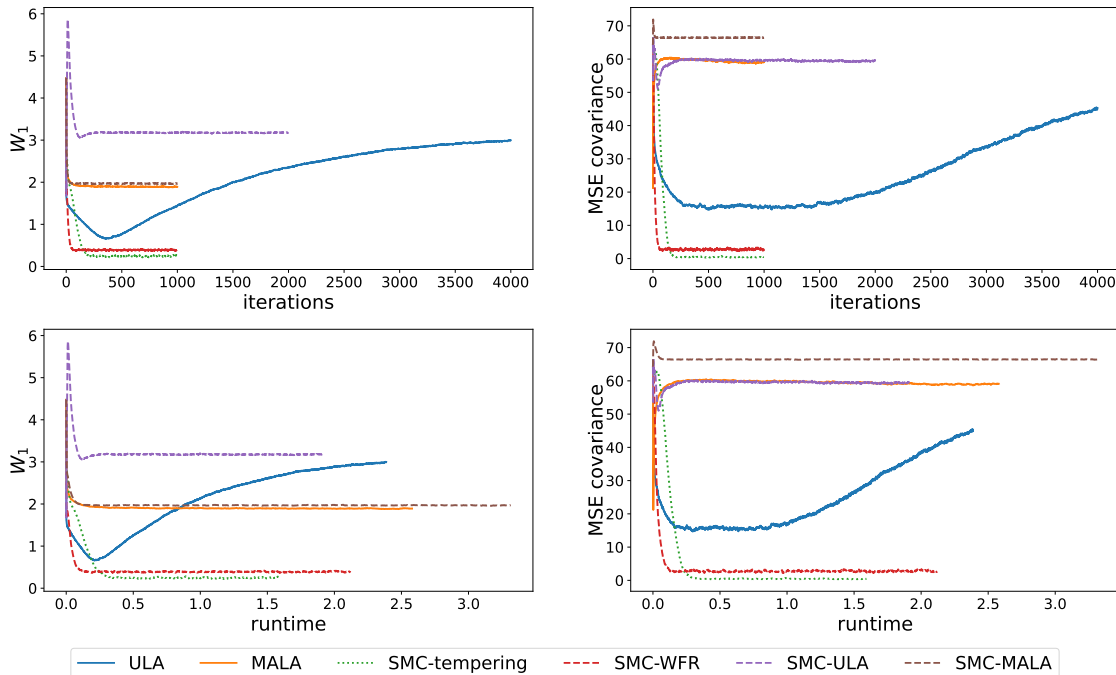


Figure 5.3: 2D Gaussian mixture: Evolution of W_1 and mean squared error (MSE) for the covariance matrix against runtime (first row) and number of iterations (second row) averaged over 50 repetitions. The initial distribution is $\mu_0(x) = \mathcal{N}(x; 0, \text{Id})$. We compare ULA, MALA, SMC tempering, SMC-WFR, SMC-ULA and SMC-MALA. SMC-WFR achieves the fastest convergence both in number of iterations and in runtime, ULA and MALA based algorithms fail to identify all the modes.

6 Conclusions

We study the connection between sampling algorithms and gradient flows in the space of probability measures, with focus on the Fisher–Rao and Wasserstein–Fisher–Rao geometry. We identify a natural parallel between Fisher–Rao dynamics and importance sampling and use this idea to propose a sequential Monte Carlo (SMC) algorithm which approximates the Wasserstein–Fisher–Rao dynamics. This algorithm has convergence guarantees (Proposition 3.1 and 3.2) and shows superior performance to other approximations (Section 5.1). In particular, Proposition 3.1 establishes that the time discretisation of the WFR PDE (2.3) used by SMC-WFR decreases the KL divergence at an exponential rate and is sharper than the decay achieved by the W flow only. Proposition 3.2 extends a classical result in the SMC literature to SMC-WFR, showing that the particle approximation obtained by replacing densities with empirical measures leads to consistent estimates with mean squared error that decays at rate $N^{-1/2}$.

Numerical approximations of the WFR flow are underexplored, and their ability to realise the theoretical gains of the WFR flow over pure W and FR flows [Lu et al., 2023] is poorly understood. We propose a numerical approximation of the WFR flow (Algorithm 1) and investigate whether this approximation maintains the superior theoretical performances of the WFR flow in (2.5). To achieve this goal, we performed a simulation study on a range of targets which exhibit different challenges (e.g. multimodality, concentration, high dimensionality) and compared the convergence speed in terms of wallclock time of Algorithm 1 with popular Monte Carlo methods. Our experiments complement the theoretical rate (2.5) taking into account numerical approximation via two popular classes of Monte Carlo methods: MCMC and importance sampling.

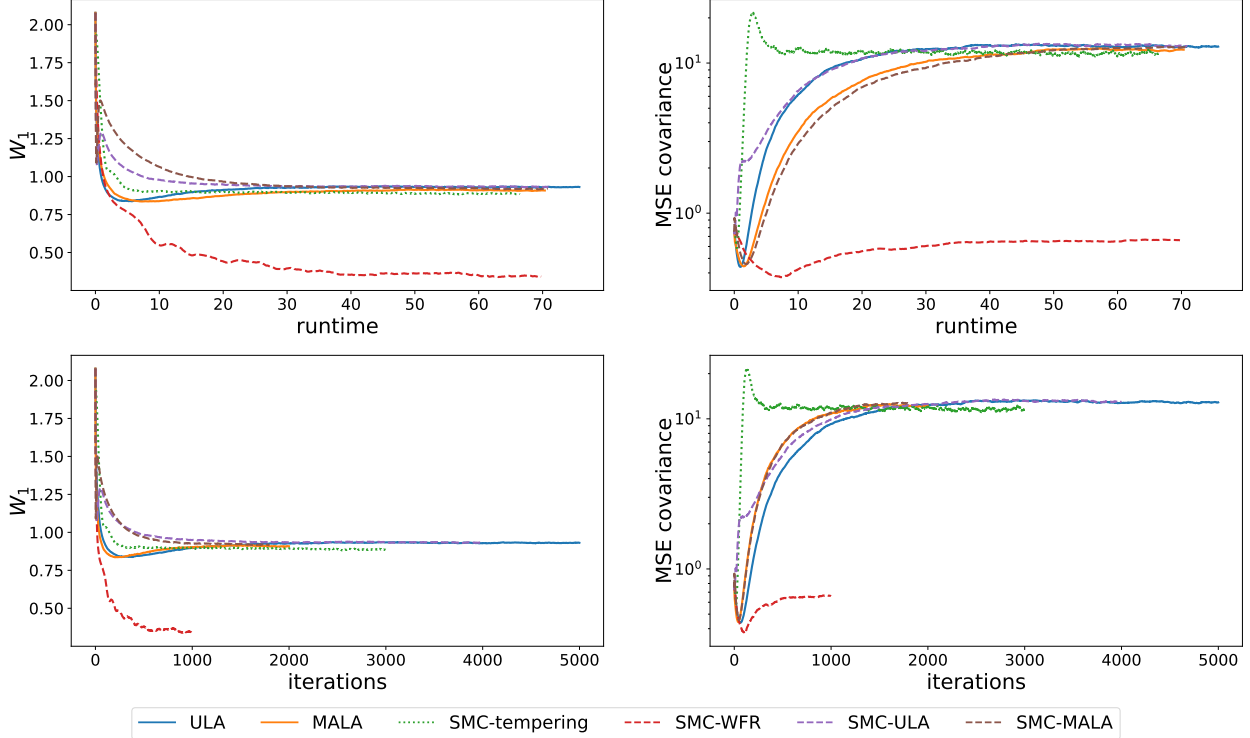


Figure 5.4: 20D Gaussian mixture: Evolution of W_1 and mean squared error (MSE) for the covariance matrix against runtime (first row) and number of iterations (second row) averaged over 50 repetitions. The initial distribution is $\mu_0(x) = \mathcal{N}(x; 0, \text{Id})$. We compare ULA, MALA, SMC tempering, SMC-WFR, SMC-ULA and SMC-MALA. SMC-WFR achieves the fastest convergence both in number of iterations and in runtime.

Interpreting SMC as the gradient flow of the KL divergence w.r.t. the Wasserstein–Fisher–Rao geometry allows us to exploit the well known results connecting Langevin dynamics to Wasserstein gradient flows of KL to gain some insight on when SMC performs better than Langevin-based algorithms. We identify the following properties of the target and initial distribution which should guide the choice of sampling algorithm to achieve the best tradeoff between accuracy and convergence speed:

- If $\pi \propto e^{-V_\pi}$ satisfies a log-Sobolev inequality (2.4) with small C_{LSI} , ∇V_π is well-behaved and μ_0 puts mass on a region of high target probability, then the W flow works well, and ULA and MALA are likely to provide good results (e.g. the donut and Gaussian examples). In this case approximating the WFR flow might be unnecessary as it will closely follow the W flow.
- In the case of large C_{LSI} or if the gradients of ∇V_π are not globally Lipschitz, the combination of the diffusive behaviour of ULA with the importance sampling approach approximating the FR step in SMC-WFR provides a considerable advantage both in terms of runtime and stability (e.g. the banana and Gaussian mixture examples).
- SMC-WFR and SMC-tempering are more robust to the choice of initial distribution and provide good results even when π and μ_0 do not significantly overlap. This is largely due to the use of tempering techniques.

We also highlight some limitations of the proposed methodology and opportunities for further developments of numerical approximations of the WFR flow that can realise its superior theoretical guarantees:

- Algorithm 1 relies on ULA for the proposal step and thus is not suited for non-differentiable targets, is unstable when ULA is and provides little exploration for targets with challenging geometry. To circumvent stability and non-differentiability issues, one could consider alternative approximations of

the Langevin diffusion [Salim et al., 2019, 2020, Mou et al., 2021]. To improve exploration, standard recipes like preconditioning [Dalalyan, 2017, Hird and Livingstone, 2025] and modulation of the diffusion coefficient could be beneficial [Pavliotis, 2014].

- The $\mathcal{O}(N^2)$ computational cost of SMC-WFR is balanced out by the improved convergence speed for small N but for large N the $\mathcal{O}(N)$ cost of the weights (3.5) might become prohibitive. This can be addressed adapting N -body learning techniques as in Klaas et al. [2005], Lang et al. [2005] or considering efficient implementations using GPUs as shown in Clarté et al. [2022, Section 4]. The use of multiple proposal steps in SMC-WFR can also mitigate computational cost as the ULA updates are cheap, but is only beneficial when ULA works well.
- SMC-WFR does not correct for the time discretisation bias of ULA. As swapping ULA for MALA as in SMC-MALA seems to deteriorate the performances of the algorithm, one could instead use adaptive stepsizes: large at first to favour fast convergence and then smaller as time goes on to reduce bias. Alternatively, one could replace SMC-WFR with SMC-MALA once SMC-WFR has converged to high target probability regions.

Nevertheless, we demonstrate that the proposed SMC based algorithm is competitive on a range of multimodal examples. We hope that the ideas in this manuscript help spur the development of further numerical approximations of WFR flows.

Acknowledgements The authors would like to thank Deniz Akyildiz, Paula Cordero Encinar, Nikolas Nüsken, Anna Korba, Linfeng Wang for helpful discussions. The authors gratefully acknowledge the mathematical research institute MATRIX in Australia where part of this research was performed.

F.R.C. is supported by the Gruppo Nazionale per l’Analisi Matematica, la Probabilità e le loro Applicazioni (GNAMPA-INdAM).

References

- Sergios Agapiou, Omiros Papaspiliopoulos, Daniel Sanz-Alonso, and Andrew M Stuart. Importance sampling: Intrinsic dimension and computational cost. *Statistical Science*, pages 405–431, 2017.
- Ömer Deniz Akyildiz. A probabilistic interpretation of replicator-mutator dynamics. *arXiv preprint arXiv:1712.07879*, 2017.
- Luigi Ambrosio, Nicola Gigli, and Giuseppe Savaré. *Gradient flows: in metric spaces and in the space of probability measures*. Springer Science & Business Media, 2008.
- Pierre-Cyril Aubin-Frankowski, Anna Korba, and Flavien Léger. Mirror descent with relative smoothness in measure spaces, with application to Sinkhorn and EM. *Advances in Neural Information Processing Systems*, 35:17263–17275, 2022.
- P. Berti, L. Pratelli, and P. Rigo. Almost sure weak convergence of random probability measures. *Stochastics and Stochastics Reports*, 78(2):91–97, 2006.
- Pascal Bianchi, Bernard Delyon, Victor Priser, and François Portier. Stochastic mirror descent for nonparametric adaptive importance sampling. *arXiv preprint arXiv: 2409.13272*, 2024.
- David M Blei, Alp Kucukelbir, and Jon D McAuliffe. Variational inference: A review for statisticians. *Journal of the American Statistical Association*, 112(518):859–877, 2017.
- A. Boustati, Ö. D. Akyildiz, T. Damoulas, and A. M. Johansen. Generalized Bayesian filtering via sequential Monte Carlo. In H. Larochelle, M. Ranzato, R. Hadsell, M. F. Balcan, and H. Lin, editors, *Advances in Neural Information Processing Systems*, volume 33, pages 418–429. Curran Associates, Inc., 2020.
- José A. Carrillo, Yifan Chen, Daniel Zhengyu Huang, Jiaoyang Huang, and Dongyi Wei. Fisher-Rao Gradient Flow: Geodesic Convexity and Functional Inequalities. *arXiv preprint arXiv:2407.15693*, 2024. arXiv:2407.15693 [math].

- Yifan Chen, Daniel Zhengyu Huang, Jiaoyang Huang, Sebastian Reich, and Andrew M Stuart. Sampling via gradient flows in the space of probability measures. *arXiv preprint arXiv:2310.03597*, 2023.
- Yifan Chen, Daniel Zhengyu Huang, Jiaoyang Huang, Sebastian Reich, and Andrew M Stuart. Efficient, multimodal, and derivative-free Bayesian inference with Fisher–Rao gradient flows. *Inverse Problems*, 40(12):125001, 2024.
- Sinho Chewi, Murat A Erdogdu, Mufan Li, Ruoqi Shen, and Matthew S Zhang. Analysis of Langevin Monte Carlo from Poincaré to log-Sobolev. *Foundations of Computational Mathematics*, pages 1–51, 2024.
- Nicolas Chopin. Central limit theorem for sequential Monte Carlo methods and its application to Bayesian inference. *The Annals of Statistics*, 32(6):2385–2411, 2004.
- Nicolas Chopin and Omri Papaspiliopoulos. *An introduction to sequential Monte Carlo*. Springer, 2020.
- Nicolas Chopin, Francesca Crucinio, and Anna Korba. A connection between tempering and entropic mirror descent. In Ruslan Salakhutdinov, Zico Kolter, Katherine Heller, Adrian Weller, Nuria Oliver, Jonathan Scarlett, and Felix Berkenkamp, editors, *Proceedings of the 41st International Conference on Machine Learning*, volume 235 of *Proceedings of Machine Learning Research*, pages 8782–8800. PMLR, 21–27 Jul 2024.
- G. Clarté, A. Diez, and J. Feydy. Collective proposal distributions for nonlinear MCMC samplers: Mean-field theory and fast implementation. *Electronic Journal of Statistics*, 22(2):6395–6460, 2022.
- D. Crisan and A. Doucet. A survey of convergence results on particle filtering methods for practitioners. *IEEE Transactions on Signal Processing*, 50(3):736–746, March 2002.
- Francesca R Crucinio and Adam M Johansen. Properties of marginal sequential Monte Carlo methods. *Statistics & Probability Letters*, 203:109914, 2023.
- Dániel Czégel, Hamza Giaffar, Joshua B. Tenenbaum, and Eörs Szathmáry. Bayes and Darwin: How replicator populations implement Bayesian computations. *BioEssays*, 44(4):1–11, 2022. ISSN 15211878. doi: 10.1002/bies.202100255.
- Bo Dai, Niao He, Hanjun Dai, and Le Song. Provable Bayesian inference via particle mirror descent. In *Artificial Intelligence and Statistics*, pages 985–994. PMLR, 2016.
- Chenguang Dai, Jeremy Heng, Pierre E Jacob, and Nick Whiteley. An invitation to sequential Monte Carlo samplers. *Journal of the American Statistical Association*, 117(539):1587–1600, 2022.
- Arnak S Dalalyan. Theoretical guarantees for approximate sampling from smooth and log-concave densities. *Journal of the Royal Statistical Society Series B: Statistical Methodology*, 79(3):651–676, 2017.
- Fred Daum and Jim Huang. Particle flow for nonlinear filters with log-homotopy. In *Signal and Data Processing of Small Targets 2008*, volume 6969, pages 414–425. SPIE, 2008.
- Pierre Del Moral. Nonlinear filtering: Interacting particle resolution. *Comptes Rendus de l’Académie des Sciences - Series I - Mathematics*, 325(1):653–658, 1997. doi: [https://doi.org/10.1016/S0764-4442\(97\)84778-7](https://doi.org/10.1016/S0764-4442(97)84778-7).
- Pierre Del Moral. *Feynman-Kac formulae: genealogical and interacting particle systems with applications*. Probability and Its Applications. Springer Verlag, New York, 2004.
- Pierre Del Moral, Arnaud Doucet, and Ajay Jasra. Sequential Monte Carlo samplers. *Journal of the Royal Statistical Society Series B: Statistical Methodology*, 68(3):411–436, 2006.
- Carles Domingo-Enrich and Aram-Alexandre Pooladian. An Explicit Expansion of the Kullback-Leibler Divergence along its Fisher-Rao Gradient Flow. *Transactions on Machine Learning Research*, 2023. ISSN 2835-8856.

- Alain Durmus, Szymon Majewski, and Błażej Miasojedow. Analysis of Langevin Monte Carlo via convex optimization. *Journal of Machine Learning Research*, 20(73):1–46, 2019.
- Víctor Elvira, Luca Martino, David Luengo García, and Mónica F Bugallo. Generalized multiple importance sampling. *Statistical Science*, 34(1):129–155, 2019.
- Akio Fujiwara and Shun-ichi Amari. Gradient systems in view of information geometry. *Physica D: Nonlinear Phenomena*, 80(3):317–327, 1995.
- Thomas O Gallouët and Leonard Monsaingeon. A JKO splitting scheme for Kantorovich–Fisher–Rao gradient flows. *SIAM Journal on Mathematical Analysis*, 49(2):1100–1130, 2017.
- Alfredo Garbuno-Inigo, Franca Hoffmann, Wuchen Li, and Andrew M Stuart. Interacting Langevin diffusions: Gradient structure and ensemble Kalman sampler. *SIAM Journal on Applied Dynamical Systems*, 19(1):412–441, 2020.
- Mathieu Gerber, Nicolas Chopin, and Nick Whiteley. Negative association, ordering and convergence of resampling methods. *Annals of Statistics*, 47(4):2236–2260, 2019.
- Charles J Geyer. Markov chain Monte Carlo maximum likelihood. In E. M. Keramides, editor, *Computing Science and Statistics: Proceedings of the 23rd Symposium on the Interface*, pages 156–163, 1991.
- N. J. Gordon, S. J. Salmond, and A. F. M. Smith. Novel approach to nonlinear/non-Gaussian Bayesian state estimation. *IEE Proceedings-F*, 140(2):107–113, 1993.
- Arthur Gretton, Karsten M Borgwardt, Malte J Rasch, Bernhard Schölkopf, and Alexander Smola. A kernel two-sample test. *Journal of Machine Learning Research*, 13(1):723–773, 2012.
- Marc Harper. Information geometry and evolutionary game theory. *arXiv preprint arXiv:0911.1383*, 2009a.
- Marc Harper. The replicator equation as an inference dynamic. *arXiv preprint arXiv:0911.1763*, 2009b.
- Max Hird and Samuel Livingstone. Quantifying the effectiveness of linear preconditioning in Markov chain Monte Carlo. *Journal of Machine Learning Research*, 26(119):1–51, 2025.
- Josef Hofbauer and Karl Sigmund. *Evolutionary games and population dynamics*. Cambridge University Press, 1998.
- Ajay Jasra, David A Stephens, Arnaud Doucet, and Theodoros Tsagaris. Inference for Lévy-driven stochastic volatility models via adaptive sequential Monte Carlo. *Scandinavian Journal of Statistics*, 38(1):1–22, 2011.
- Richard Jordan, David Kinderlehrer, and Felix Otto. The variational formulation of the Fokker–Planck equation. *SIAM Journal on Mathematical Analysis*, 29(1):1–17, 1998.
- M. Klaas, N. de Freitas, and A. Doucet. Towards practical N^2 Monte Carlo: The marginal particle filter. In *Proceedings of Uncertainty in Artificial Intelligence*, pages 308–315, 2005.
- Anna Korba and François Portier. Adaptive importance sampling meets mirror descent: a bias-variance tradeoff. In *International Conference on Artificial Intelligence and Statistics*, pages 11503–11527. PMLR, 2022.
- Marc Lambert, Sinho Chewi, Francis Bach, Silvère Bonnabel, and Philippe Rigollet. Variational inference via Wasserstein gradient flows. *Advances in Neural Information Processing Systems*, 35:14434–14447, 2022.
- D. Lang, M. Klaas, and N. de Freitas. Empirical testing of fast kernel density estimation algorithms. *Technical Report TR2005-03, Department of Computer Science, University of British Columbia*, 2005.
- Matthias Liero, Alexander Mielke, Oliver Tse, and Jia-Jie Zhu. Evolution of Gaussians in the Hellinger-Kantorovich-Boltzmann gradient flow. *arXiv preprint arXiv:2504.20400*, 2025.
- Qiang Liu and Dilin Wang. Stein variational gradient descent: A general purpose Bayesian inference algorithm. *Advances in Neural Information Processing Systems*, 29, 2016.

- Yulong Lu, Jianfeng Lu, and James Nolen. Accelerating Langevin Sampling with Birth-death. *arXiv preprint arXiv: 1905.09863*, pages 1–18, 2019.
- Yulong Lu, Dejan Slepcev, and Lihan Wang. Birth-death dynamics for sampling: Global convergence, approximations and their asymptotics. *Nonlinearity*, 36(11):5731–5772, 2023. ISSN 0951-7715, 1361-6544.
- Aimee Maurais and Youssef Marzouk. Sampling in unit time with kernel Fisher-rao flow. In Ruslan Salakhutdinov, Zico Kolter, Katherine Heller, Adrian Weller, Nuria Oliver, Jonathan Scarlett, and Felix Berkenkamp, editors, *Proceedings of the 41st International Conference on Machine Learning*, volume 235 of *Proceedings of Machine Learning Research*, pages 35138–35162. PMLR, 21–27 Jul 2024.
- Wenlong Mou, Yi-An Ma, Martin J Wainwright, Peter L Bartlett, and Michael I Jordan. High-order Langevin diffusion yields an accelerated MCMC algorithm. *Journal of Machine Learning Research*, 22(1):1919–1959, 2021.
- Radford M Neal. Annealed importance sampling. *Statistics and Computing*, 11:125–139, 2001.
- Nikolas Nüsken. Stein Transport for Bayesian Inference. *arXiv preprint arXiv:2409.01464*, 2024.
- Jimmy Olsson and Tobias Rydén. The bootstrap particle filtering bias. *Lund University, Technical Report 929081*, 2004.
- Benjamin Pampel, Simon Holbach, Lisa Hartung, and Omar Valsson. Sampling rare event energy landscapes via birth-death augmented dynamics. *Physical Review E*, 107(2):024141, 2023.
- Sahani Pathiraja and Philipp Wacker. Connections between sequential Bayesian inference and evolutionary dynamics. *Philosophical Transactions of the Royal Society A: Mathematical, Physical and Engineering Sciences (accepted)*, 2024. doi: 10.1098/rsta.2024.0241.
- Grigorios A. Pavliotis. *The Langevin Equation*, chapter Chapter 6, pages 181–233. Springer New York, New York, NY, 2014. ISBN 978-1-4939-1323-7. doi: 10.1007/978-1-4939-1323-7_6.
- Gareth O Roberts and Jeffrey S Rosenthal. Optimal scaling for various Metropolis-Hastings algorithms. *Statistical Science*, 16(4):351–367, 2001.
- Gareth O Roberts and Richard L Tweedie. Exponential convergence of Langevin distributions and their discrete approximations. *Bernoulli*, pages 341–363, 1996.
- Adil Salim, Dmitry Kovalev, and Peter Richtarik. Stochastic proximal Langevin algorithm: Potential splitting and nonasymptotic rates. In H. Wallach, H. Larochelle, A. Beygelzimer, F. d'Alché-Buc, E. Fox, and R. Garnett, editors, *Advances in Neural Information Processing Systems*, volume 32. Curran Associates, Inc., 2019.
- Adil Salim, Anna Korba, and Giulia Luise. The Wasserstein proximal gradient algorithm. *Advances in Neural Information Processing Systems*, 33:12356–12366, 2020.
- André Schlichting. Poincaré and log-Sobolev inequalities for mixtures. *Entropy*, 21(1):89, 2019.
- S. M. Schmon, G. Deligiannidis, A. Doucet, and M. K. Pitt. Large sample asymptotics of the pseudo-marginal method. *Biometrika*, 108(1):37–51, 2021.
- Cosma Rohilla Shalizi. Dynamics of Bayesian updating with dependent data and misspecified models. *Electronic Journal of Statistics*, 3:1039–1074, 2009. ISSN 19357524. doi: 10.1214/09-EJS485.
- Saifuddin Syed, Alexandre Bouchard-Côté, Kevin Chern, and Arnaud Doucet. Optimised annealed sequential Monte Carlo samplers. *arXiv preprint arXiv:2408.12057*, 2024.
- Santosh Vempala and Andre Wibisono. Rapid convergence of the unadjusted langevin algorithm: Isoperimetry suffices. In H. Wallach, H. Larochelle, A. Beygelzimer, F. d'Alché-Buc, E. Fox, and R. Garnett, editors, *Advances in Neural Information Processing Systems*, volume 32. Curran Associates, Inc., 2019.

Linfeng Wang and Nikolas Nüsken. Measure transport with kernel mean embeddings. *arXiv preprint arXiv:2401.12967*, pages 1–21, 2024.

Andre Wibisono. Sampling as optimization in the space of measures: The Langevin dynamics as a composite optimization problem. In *Conference on Learning Theory*, pages 2093–3027. PMLR, 2018.

Yuling Yan, Kaizheng Wang, and Philippe Rigollet. Learning Gaussian mixtures using the Wasserstein–Fisher–Rao gradient flow. *Annals of Statistics*, 52(4):1774–1795, 2024.

A Supplementary Lemmata

Lemma A.1. *Let ρ_t denote an unnormalised probability density function, and assume its time evolution is governed by*

$$\partial_t \rho_t(x) = \rho_t(x) f(x) \quad (\text{A.1})$$

for some function $f(x)$, also known as the “fitness function” in the evolutionary biology literature. The evolution of the normalised probability density $\mu_t(x) = \frac{\rho_t(x)}{\int \rho_t(y) dy}$ is given by the replicator PDE

$$\partial_t \mu_t(x) = \mu_t(x) (f(x) - \mathbb{E}_{\mu_t}[f]) \quad (\text{A.2})$$

Proof. Differentiating the expression for $\mu_t(x)$ with respect to t and substituting in (A.1),

$$\begin{aligned} \partial_t \mu_t(x) &= \frac{\partial_t \rho_t(x)}{\int \rho_t(y) dy} - \frac{\rho_t(x)}{(\int \rho_t(y) dy)^2} \int \partial_t \rho_t(y) dy \\ &= \frac{\rho_t(x) f(x)}{\int \rho_t(y) dy} - \frac{\rho_t(x)}{(\int \rho_t(y) dy)^2} \int f(y) \rho_t(y) dy \\ &= \mu_t(x) f(x) - \mu_t(x) \int f(y) \mu_t(y) dy \end{aligned}$$

yields the desired result. \square

Lemma A.2 (Unit time FR as a deterministic time rescaling of infinite time FR.). *Consider the unit time FR PDE*

$$\partial_t \mu_t(x) = \mu_t(x) \log \left(\frac{\pi(x)}{\mu_0(x)} \right) - \mathbb{E}_{\mu_t} \left[\frac{\pi(x)}{\mu_0(x)} \right], \quad t \in [0, 1] \quad (\text{A.3})$$

Let $\mu_\tau^* = \mu_t$ where $\tau = -\log(1-t)$ and μ_t is a solution of (A.3). Then formally, μ_τ^* is a solution of the infinite time FR PDE

$$\partial_t \mu_\tau^*(x) = \mu_\tau^*(x) \log \left(\frac{\pi(x)}{\mu_\tau^*(x)} \right) - \mathbb{E}_{\mu_\tau^*} \left[\frac{\pi(x)}{\mu_\tau^*(x)} \right], \quad \tau \in [0, \infty)$$

Proof. Consider the geometric interpolation

$$\rho_t(x) = \pi^t(x) \rho_0^{1-t}(x) = \exp[t \log \pi(x) + (1-t) \log \rho_0(x)] \quad (\text{A.4})$$

where ρ_t denotes an unnormalised probability density. Differentiating both sides with respect to t yields

$$\partial_t \rho_t = \rho_t(x) \log \left(\frac{\pi(x)}{\rho_0(x)} \right), \quad t \in [0, 1], \quad (\text{A.5})$$

that is, the unit time Fisher–Rao PDE in unnormalised form (see Lemma A.1). Consider the deterministic time change $\tau = -\log(1-t)$ where $\tau \in [0, \infty)$ such that $\rho_\tau^* = \rho_t$. Then using (A.4),

$$\log \rho_\tau^* = \log \rho_{t(\tau)} = (1 - \exp(-\tau)) \log \pi + \exp(-\tau) \log \rho_0 \quad (\text{A.6})$$

and $\frac{dt}{d\tau} = \exp(-\tau)$. Combining these results and applying chain rule to (A.5),

$$\begin{aligned} \partial_\tau \rho_\tau^* &= \frac{dt}{d\tau} \partial_t \rho_{t(\tau)} = \exp(-\tau) \rho_{t(\tau)} \log \left(\frac{\pi}{\rho_0} \right) \\ &= \rho_{t(\tau)} [\exp(-\tau) \log \pi - \exp(-\tau) \log \rho_0] \\ &= \rho_\tau^* [\exp(-\tau) \log \pi - \exp(-\tau) \log \rho_0] \\ &= \rho_\tau^* [\exp(-\tau) \log \pi + (1 - \exp(-\tau)) \log \pi - \log \rho_\tau^*] \\ &= \rho_\tau^* [\log \pi - \log \rho_\tau^*] \end{aligned}$$

yields the unnormalised form of the infinite time FR PDE. Applying the normalisation Lemma A.1 yields the result. \square

B Proof of Proposition 3.1

Proof. Let us denote $\mathcal{F}(\mu) = \text{KL}(\mu|\pi)$. To show that the mirror descent update (3.3) reduces \mathcal{F} we reproduce the argument of Chopin et al. [2024, Proposition 1]. Since \mathcal{F} is 1-relatively smooth with respect to $\phi : \mu \mapsto \int \log(\mu(x))d\mu(x)$ [Aubin-Frankowski et al., 2022] and since $\delta = 1 - e^{-\gamma} \leq 1$, for all $\gamma > 0$, we have

$$\begin{aligned} \mathcal{F}(\mu_n) &\leq \mathcal{F}(\mu_{n-1/2}) + \langle \nabla \mathcal{F}(\mu_{n-1/2}), \mu_n - \mu_{n-1/2} \rangle + B_\phi(\mu_n|\mu_{n-1/2}) \\ &\leq \mathcal{F}(\mu_{n-1/2}) + \langle \nabla \mathcal{F}(\mu_{n-1/2}), \mu_n - \mu_{n-1/2} \rangle + \frac{1}{\delta} B_\phi(\mu_n|\mu_{n-1/2}), \end{aligned} \quad (\text{B.1})$$

where $B_\phi(\nu|\mu) = \phi(\nu) - \phi(\mu) - \langle \nabla \phi(\mu), \nu - \mu \rangle$ denotes the Bregman divergence and $\nabla \phi$ the first variation. Applying Aubin-Frankowski et al. [2022, Lemma 3] to the convex function $G(\nu) = \delta \langle \nabla \mathcal{F}(\mu_{n-1/2}), \nu - \mu_{n-1/2} \rangle$, with $\mu = \mu_{n-1/2}$ and $\bar{\nu} = \mu_n$ yields

$$\begin{aligned} \langle \nabla \mathcal{F}(\mu_{n-1/2}), \mu_n - \mu_{n-1/2} \rangle + \frac{1}{\delta} B_\phi(\mu_n|\mu_{n-1/2}) &\leq \\ \langle \nabla \mathcal{F}(\mu_{n-1}), \nu - \mu_{n-1/2} \rangle + \frac{1}{\delta} B_\phi(\nu|\mu_{n-1/2}) - \frac{1}{\delta} B_\phi(\nu|\mu_n). \end{aligned}$$

Fix ν , then (B.1) becomes:

$$\mathcal{F}(\mu_n) \leq \mathcal{F}(\mu_{n-1/2}) + \langle \nabla \mathcal{F}(\mu_{n-1/2}), \nu - \mu_{n-1/2} \rangle + \frac{1}{\delta} B_\phi(\nu|\mu_{n-1/2}) - \frac{1}{\delta} B_\phi(\nu|\mu_n).$$

This shows in particular, by substituting $\nu = \mu_{n-1/2}$ and since $B_\phi(\nu|\mu_n) \geq 0$, that

$$\mathcal{F}(\mu_n) \leq \mathcal{F}(\mu_{n-1/2}) - \frac{1}{\delta} B_\phi(\mu_{n-1/2}|\mu_n).$$

We now show that $B_\phi(\mu_{n-1/2}|\mu_n) = \text{KL}(\mu_{n-1/2}|\mu_n) > 0$. Since B_ϕ is a divergence we know that $B_\phi(\mu_{n-1/2}|\mu_n) = 0$ iff $\mu_{n-1/2} = \mu_n$. Under the condition $\gamma > 0$, the only possibility to have $\mu_{n-1/2} = \mu_n$ is for $\mu_{n-1/2} \equiv \mu_n \equiv \pi$ for which $\mathcal{F}(\mu_{n-1/2}) = \mathcal{F}(\mu_n) = 0$. Since n is arbitrary, this implies $\mu_0 = \pi$ and thus no FR step is needed.

It follows that

$$\mathcal{F}(\mu_n) < \mathcal{F}(\mu_{n-1/2}). \quad (\text{B.2})$$

To deal with the W flow update we observe that $\mu_{n-1/2}$ in (3.4) with fixed is obtained as

$$\mu_{n-1/2}(x) = \mu_{n-1} R_\gamma(x) := (4\pi\gamma)^{-d/2} \int \exp\left(-\frac{1}{4\gamma} \|x - y - \gamma \nabla \log \pi(y)\|^2\right) \mu_{n-1}(y) dy$$

and using Vempala and Wibisono [2019, Lemma 3]

$$\mathcal{F}(\mu_{n-1/2}) \leq e^{-\gamma/C_{\text{LSI}}} \mathcal{F}(\mu_{n-1}) + 6\gamma^2 dL_\pi^2,$$

with $\gamma \leq C_{\text{LSI}}^{-1}/(4L_\pi^2)$. Using (B.2) and the result above we obtain

$$\mathcal{F}(\mu_n) < e^{-\gamma/C_{\text{LSI}}} \mathcal{F}(\mu_{n-1}) + 6\gamma^2 dL_\pi^2.$$

Proceeding by induction we then find that

$$\begin{aligned} \mathcal{F}(\mu_n) &< e^{-n\gamma/C_{\text{LSI}}} \mathcal{F}(\mu_0) + 6\gamma^2 dL_\pi^2 \sum_{k=0}^{n-1} e^{-k\gamma/C_{\text{LSI}}} \\ &< e^{-n\gamma/C_{\text{LSI}}} \mathcal{F}(\mu_0) + 6\gamma^2 dL_\pi^2 \left(\frac{1 - e^{-(n-1)\gamma/C_{\text{LSI}}}}{1 - e^{-\gamma/C_{\text{LSI}}}} \right) \\ &< e^{-n\gamma/C_{\text{LSI}}} \mathcal{F}(\mu_0) + 6\gamma^2 dL_\pi^2 \left(\frac{1}{1 - e^{-\gamma/C_{\text{LSI}}}} \right) \\ &< e^{-n\gamma/C_{\text{LSI}}} \mathcal{F}(\mu_0) + 8\gamma dL_\pi^2 C_{\text{LSI}}^{-1}, \end{aligned}$$

where for the last inequality we used the fact that $\gamma \leq C_{\text{LSI}}^{-1}/(4L_\pi^2) \leq C_{\text{LSI}}/4$ as in Vempala and Wibisono [2019, Theorem 1]. \square

C Proofs of Section 3.2

C.1 Preliminary definitions

For any distribution η and any $\varphi \in \mathcal{B}_b(\mathbb{R}^d)$ we denote $\eta(\varphi) := \int \varphi(x)\eta(x)dx$, similarly for all empirical distributions $\eta^N := N^{-1} \sum_{i=1}^N \delta_{X^i}$ we denote the corresponding average by $\eta^N(\varphi) := N^{-1} \sum_{i=1}^N \varphi(X^i)$.

We recall that the initial distribution is μ_0 , $\mu_{n-1/2}$ denotes the distribution after application of the W flow over time step γ and μ_n the distribution obtained by applying the FR flow over time step γ to $\mu_{n-1/2}$. The particle approximations obtained with Algorithm 1 are as follows: the particle approximation to $\mu_{n-1/2}$ is denoted by $\mu_{n-1/2}^N = N^{-1} \sum_{i=1}^N \delta_{X_n^i}$, $\mu_n^N = \sum_{i=1}^N W_n^i \delta_{X_n^i}$ and $\tilde{\mu}_n^N = N^{-1} \sum_{i=1}^N \delta_{\tilde{X}_n^i}$ both approximate μ_n .

C.2 Control of FR flow approximation

To control the error introduced by the weighting step we first consider the idealised algorithm in which $\mu_{n-1/2}$ can be computed analytically and the weights are given by

$$v_n(x) = \left(\frac{\pi(x)}{\mu_{n-1/2}(x)} \right)^{1-e^{-\gamma}}.$$

We then compare the evolution of this algorithm with that of Algorithm 1 and show that the additional approximation in the weights does not alter the rate in the error bounds.

Before moving forward, we recall the following standard representation of importance sampling estimators:

$$\mu_n^N(\varphi) = \sum_{i=1}^N W_n^i \varphi(X_n^i) = \frac{\sum_{i=1}^N w_n(X_n^i) \varphi(X_n^i)}{\sum_{i=1}^N w_n(X_n^i)} = \frac{\mu_{n-1/2}^N(w_n \varphi)}{\mu_{n-1/2}^N(w_n)}$$

and

$$\begin{aligned} \mu_n(\varphi) &= \frac{\int \mu_{n-1/2}(x) e^{-\gamma} \pi(x)^{1-e^{-\gamma}} \varphi(x) dx}{\int \mu_{n-1/2}(x) e^{-\gamma} \pi(x)^{1-e^{-\gamma}} dx} \\ &= \frac{\int \mu_{n-1/2}(x) \varphi(x) \left(\frac{\pi(x)}{\mu_{n-1/2}(x)} \right)^{1-e^{-\gamma}} dx}{\int \mu_{n-1/2}(x) \left(\frac{\pi(x)}{\mu_{n-1/2}(x)} \right)^{1-e^{-\gamma}} dx} = \frac{\mu_{n-1/2}(v_n \varphi)}{\mu_{n-1/2}(v_n)}. \end{aligned} \tag{C.1}$$

Key to the following results is the following Proposition which obtains the conditional expectations of $\mu_{n-1/2}^N(w_n \varphi)$ and closely follows the result in Crucinio and Johansen [2023, Proposition 7].

Proposition C.1. *Let \mathcal{F}_{n-1}^N denote the σ -field generated by the weighted samples up to (and including) time $n-1$ and let us define $M_n(x_{n-1}, \cdot) := \mathcal{N}(\cdot; x_{n-1} + \gamma \nabla \log \pi(x_{n-1}), 2\gamma \cdot \mathbf{Id})$.*

We have

$$\mathbb{E} \left[\mu_{n-1/2}^N(w_n \varphi) \mid \mathcal{F}_{n-1}^N \right] = \int \varphi(x_n) \pi(x_n)^{1-e^{-\gamma}} \left(\mu_{n-1/2}^N(x_n) \right)^{e^{-\gamma}} dx_n,$$

for all $n \geq 1$ and all $\varphi \in \mathcal{B}_b(\mathbb{R}^d)$. In addition,

$$\mu_{n-1/2}(v_n \varphi) = \int \varphi(x_n) \pi(x_n)^{1-e^{-\gamma}} \left(\mu_{n-1/2}(x_n) \right)^{e^{-\gamma}} dx_n.$$

Proof. Let us denote the σ -field generated by the particle system up to (and including) time $n-1$ before the W flow at time n by $\mathcal{G}_{n-1}^N := \sigma \left(\tilde{X}_{n-1}^i : i \in \{1, \dots, N\} \right) \vee \mathcal{F}_{n-1}^N$.

Consider the conditional expectation

$$\begin{aligned}
\mathbb{E} \left[\mu_{n-1/2}^N(w_n \varphi) \mid \mathcal{F}_{n-1}^N \right] &= \frac{1}{N} \sum_{i=1}^N \mathbb{E} \left[w_n(X_n^i) \varphi(X_n^i) \mid \mathcal{F}_{n-1}^N \right] \\
&= \frac{1}{N} \sum_{i=1}^N \mathbb{E} \left[\mathbb{E} \left[w_n(X_n^i) \varphi(X_n^i) \mid \mathcal{G}_{n-1}^N \right] \mid \mathcal{F}_{n-1}^N \right] \\
&= \frac{1}{N} \sum_{i=1}^N \mathbb{E} \left[\int M_n(\tilde{X}_{n-1}^i, dx_n) w_n(x_n) \varphi(x_n) \mid \mathcal{F}_{n-1}^N \right] \\
&= \sum_{j=1}^N \frac{w_{n-1}^N(X_{n-1}^j)}{\sum_{k=1}^N w_{n-1}^N(X_{n-1}^k)} \int M_n(X_{n-1}^j, x_n) w_n(x_n) \varphi(x_n) dx_n,
\end{aligned}$$

where the third equality follows from the fact that $X_n^i \mid \mathcal{G}_{n-1}^N \sim M_n(\tilde{X}_{n-1}^i, \cdot)$ for each $i = 1, \dots, N$ and the fourth from the fact that $\{X_{n-1}^j\}_{j=1}^N$ and w_{n-1} are \mathcal{F}_{n-1}^N -measurable and conditionally each \tilde{X}_{n-1}^i is drawn independently from the categorical distribution with probabilities given by the weights.

Plugging the definition of w_n into the above and observing that

$$\begin{aligned}
\mu_{n-1/2}^N(x_n) &= \sum_{i=1}^N W_{n-1}^i M_n(X_{n-1}^i, x_n) \\
&= \sum_{i=1}^N \frac{w_{n-1}(X_{n-1}^i)}{\sum_{k=1}^N w_{n-1}(X_{n-1}^k)} M_n(X_{n-1}^i, x_n)
\end{aligned}$$

we obtain

$$\begin{aligned}
&\mathbb{E} \left[\mu_{n-1/2}^N(w_n \varphi) \mid \mathcal{F}_{n-1}^N \right] \\
&= \sum_{j=1}^N \frac{w_{n-1}(X_{n-1}^j)}{\sum_{k=1}^N w_{n-1}(X_{n-1}^k)} \int M_n(X_{n-1}^j, x_n) \varphi(x_n) \left(\frac{\pi(x_n)}{\mu_{n-1/2}^N(x_n)} \right)^{1-e^{-\gamma}} dx_n \\
&= \int \varphi(x_n) \left(\mu_{n-1/2}^N(x_n) \right)^{e^{-\gamma}} \pi(x_n)^{1-e^{-\gamma}} dx_n.
\end{aligned}$$

The second result follows from (C.1). □

The following result shows that as $N \rightarrow \infty$ the weights w_n converge to those of the idealised algorithm.

Proposition C.2. *Assume that for any $\varphi \in \mathcal{B}_b(\mathbb{R}^d)$ and any $p \geq 1$ there exists some finite constant $C_{p,n-1}(\gamma)$ such that*

$$\mathbb{E} \left[\left| \tilde{\mu}_{n-1}^N(\varphi) - \mu_{n-1}(\varphi) \right|^p \right]^{1/p} \leq C_{p,n-1}(\gamma) \frac{\|\varphi\|_\infty}{N^{1/2}}.$$

Under the conditions of Proposition 3.2, we have for any $p \geq 1$ and some finite constant $D_{p,n}(\gamma)$

$$\mathbb{E} \left[\left| \mu_{n-1/2}^N(x_n)^{e^{-\gamma}} - \mu_{n-1/2}(x_n)^{e^{-\gamma}} \right|^p \right]^{1/p} \leq \frac{D_{p,n}(\gamma)}{N^{1/2}}.$$

Proof. Consider a Taylor expansion of the function $u \mapsto u^\delta$ with $\delta = e^{-\gamma} > 0$ around u_0 with a second order remainder of Lagrange form

$$u^\delta = u_0^\delta + \delta u_0^{\delta-1} (u - u_0) + \delta(\delta - 1) \theta_u^{\delta-2} (u - u_0)^2$$

where θ_u is a point between u and u_0 . Applying this Taylor expansion with to $\mu_{n-1/2}^N(x_n)^\delta$ around the point $\mu_{n-1/2}(x_n)$ gives

$$\begin{aligned} \mu_{n-1/2}^N(x_n)^\delta - \mu_{n-1/2}(x_n)^\delta &= \delta \mu_{n-1/2}(x_n)^{\delta-1} \left(\mu_{n-1/2}^N(x_n) - \mu_{n-1/2}(x_n) \right) \\ &\quad + \delta(\delta-1) \theta_u^{\delta-2} \left(\mu_{n-1/2}^N(x_n) - \mu_{n-1/2}(x_n) \right)^2 \end{aligned} \quad (\text{C.2})$$

where θ_u is a point between $\mu_{n-1/2}^N(x_n)$ and $\mu_{n-1/2}(x_n)$. It follows that

$$\begin{aligned} \mathbb{E} \left[\left| \mu_{n-1/2}^N(x_n)^\delta - \mu_{n-1/2}(x_n)^\delta \right|^p \right]^{1/p} &\leq \delta \mu_{n-1/2}(x_n)^{\delta-1} \mathbb{E} \left[\left| \mu_{n-1/2}^N(x_n) - \mu_{n-1/2}(x_n) \right|^p \right]^{1/p} \\ &\quad + \delta |\delta-1| \mathbb{E} \left[\theta_u^{p(\delta-2)} \left| \mu_{n-1/2}^N(x_n) - \mu_{n-1/2}(x_n) \right|^{2p} \right]^{1/p}. \end{aligned}$$

Notice that θ_u is random since $\mu_{n-1/2}^N(x_n)$ is random; in addition

$$\mu_{n-1/2}^N(x_n) = \pi(x_n)/w_n(x_n)^{1/(1-\delta)} \quad \text{and} \quad \mu_{n-1/2}(x_n) = \pi(x_n)/v_n(x_n)^{1/(1-\delta)}.$$

Under our assumptions

$$\mu_{n-1/2}^N(x_n) \geq \pi(x_n)/\|w_n\|_\infty^{1/(1-\delta)} \quad \text{and} \quad \mu_{n-1/2}(x_n) \geq \pi(x_n)/\|v_n\|_\infty^{1/(1-\delta)}.$$

It follows that

$$\theta_u \geq \pi(x_n) \max\{\|w_n\|_\infty^{-1/(1-\delta)}, \|v_n\|_\infty^{-1/(1-\delta)}\} := \beta$$

almost surely.

Therefore, since $\delta-2 = e^{-\gamma} - 2 < 0$ as $\gamma > 0$

$$\begin{aligned} \mathbb{E} \left[\left| \mu_{n-1/2}^N(x_n)^\delta - \mu_{n-1/2}(x_n)^\delta \right|^p \right]^{1/p} &\leq \delta \mu_{n-1/2}(x_n)^{\delta-1} \mathbb{E} \left[\left| \mu_{n-1/2}^N(x_n) - \mu_{n-1/2}(x_n) \right|^p \right]^{1/p} \\ &\quad + \delta |\delta-1| \beta^{\delta-2} \mathbb{E} \left[\left| \mu_{n-1/2}^N(x_n) - \mu_{n-1/2}(x_n) \right|^{2p} \right]^{1/p}. \end{aligned}$$

Recalling that $\mu_{n-1/2}^N(x_n) = \tilde{\mu}_{n-1}^N(M_n(\cdot, x_n))$ with $M_n(x_{n-1}, x_n) = \mathcal{N}(x_n; x_{n-1} + \gamma \nabla \log \pi(x_{n-1}), 2\gamma \cdot \text{Id})$ a bounded function of x_{n-1} with maximum $(4\pi\gamma)^{-d/2}$, the hypothesis then gives us

$$\begin{aligned} \mathbb{E} \left[\left| \mu_{n-1/2}^N(x_n)^\delta - \mu_{n-1/2}(x_n)^\delta \right|^p \right]^{1/p} &\leq \delta \mu_{n-1/2}(x_n)^{\delta-1} C_{p,n-1} \frac{(4\pi\gamma)^{-d/2}}{N^{1/2}} \\ &\quad + \delta |\delta-1| \beta^{\delta-2} C_{p,n-1}^2 \frac{(4\pi\gamma)^{-d}}{N}. \end{aligned}$$

□

C.3 Proof of Proposition 3.2

We proceed by induction, taking $n=0$ as the base case. At time $n=0$, the particles $(X_0^i)_{i=1}^N$ are sampled i.i.d. from μ_0 , hence $\mathbb{E}[\varphi(X_0^i)] = \mu_0(\varphi)$ for $i=1, \dots, N$. We can define the sequence of functions $\Delta_0^i: \mathbb{R}^d \mapsto \mathbb{R}$ for $i=1, \dots, N$

$$\Delta_0^i(x) := \varphi(x) - \mathbb{E}[\varphi(X_0^i)]$$

so that,

$$\mu_0^N(\varphi) - \mu_0(\varphi) = \frac{1}{N} \sum_{i=1}^N \Delta_0^i(X_0^i),$$

and apply Lemma C.3 to get for every $p \geq 1$

$$\begin{aligned}
\sqrt{N}\mathbb{E} [|\mu_0^N(\varphi) - \mu_0(\varphi)|^p]^{1/p} &\leq b(p)^{1/p} \frac{1}{\sqrt{N}} \left(\sum_{i=1}^N (\sup(\Delta_0^i) - \inf(\Delta_0^i))^2 \right)^{1/2} \\
&\leq b(p)^{1/p} \frac{1}{\sqrt{N}} \left(\sum_{i=1}^N 4 (\sup |\Delta_0^i|)^2 \right)^{1/2} \\
&\leq b(p)^{1/p} \frac{1}{\sqrt{N}} \left(\sum_{i=1}^N 16 \|\varphi\|_\infty^2 \right)^{1/2} \\
&\leq 4b(p)^{1/p} \|\varphi\|_\infty,
\end{aligned} \tag{C.3}$$

from which the result at $n = 0$ follows and the base case is established.

Lemma C.4 and C.5 below show that if the result holds at time $n - 1$ then it also holds at time n . We then conclude the proof using induction.

C.4 Auxiliary results for the proof of Proposition 3.2

As a preliminary we reproduce part of Del Moral [2004, Lemma 7.3.3], a Marcinkiewicz-Zygmund-type inequality of which we will make extensive use.

Lemma C.3 (Del Moral, 2004). *Given a sequence of probability measures $(\mu_i)_{i \geq 1}$ on a given measurable space (E, \mathcal{E}) and a collection of independent random variables, one distributed according to each of those measures, $(X_i)_{i \geq 1}$, where $\forall i, X_i \sim \mu_i$, together with any sequence of measurable functions $(h_i)_{i \geq 1}$ such that $\mu_i(h_i) = 0$ for all $i \geq 1$, we define for any $N \in \mathbb{N}$,*

$$m_N(X)(h) = \frac{1}{N} \sum_{i=1}^N h_i(X_i) \quad \text{and} \quad \sigma_N^2(h) = \frac{1}{N} \sum_{i=1}^N (\sup(h_i) - \inf(h_i))^2.$$

If the h_i have finite oscillations (i.e., $\sup(h_i) - \inf(h_i) < \infty \forall i \geq 1$) then we have:

$$\sqrt{N}\mathbb{E} [|m_N(X)(h)|^p]^{1/p} \leq b(p)^{1/p} \sigma_N(h),$$

with, for any pair of integers q, p such that $q \geq p \geq 1$, denoting $(q)_p = q!/(q-p)!$:

$$b(2q) = (2q)_q 2^{-q} \quad \text{and} \quad b(2q-1) = \frac{(2q-1)_q}{\sqrt{q-\frac{1}{2}}} 2^{-(q-\frac{1}{2})}. \tag{C.4}$$

To control the error introduced by the FR reweighting step we use standard techniques from the importance sampling literature (e.g. Crisan and Doucet [2002, Lemma 4]).

Lemma C.4 (FR flow). *Under the conditions of Proposition 3.2, assume that for $p \geq 1$ and some finite constant $C_{p,n}$*

$$\mathbb{E} [|\tilde{\mu}_{n-1}^N(\varphi) - \mu_{n-1}(\varphi)|^p]^{1/p} \leq C_{p,n-1}(\gamma) \frac{\|\varphi\|_\infty}{N^{1/2}}.$$

then

$$\mathbb{E} [|\mu_n^N(\varphi) - \mu_n(\varphi)|^p]^{1/p} \leq \tilde{C}_{p,n}(\gamma) \frac{\|\varphi\|_\infty}{N^{1/2}}$$

for any $\varphi \in \mathcal{B}_b(\mathbb{R}^d)$ and any $p \geq 1$.

Proof. Let us assume that

$$\mathbb{E} \left[|\mu_{n-1/2}^N(w_n \varphi) - \mu_{n-1/2}(v_n \varphi)|^p \right]^{1/p} \leq \tilde{C}_{p,n} \frac{\|\varphi\|_\infty}{N^{1/2}} \tag{C.5}$$

for $p \geq 1$ and finite constant $\tilde{C}_{p,n}(\gamma)$. Apply the definition of μ_n and μ_n^N and consider the following decomposition

$$\begin{aligned} |\mu_n^N(\varphi) - \mu_n(\varphi)| &= \left| \frac{\mu_{n-1/2}^N(w_n\varphi)}{\mu_{n-1/2}^N(w_n)} - \frac{\mu_{n-1/2}(v_n\varphi)}{\mu_{n-1/2}(v_n)} \right| \\ &\leq \left| \frac{\mu_{n-1/2}^N(w_n\varphi)}{\mu_{n-1/2}^N(w_n)} - \frac{\mu_{n-1/2}^N(w_n\varphi)}{\mu_{n-1/2}(v_n)} \right| + \left| \frac{\mu_{n-1/2}^N(w_n\varphi)}{\mu_{n-1/2}(v_n)} - \frac{\mu_{n-1/2}(v_n\varphi)}{\mu_{n-1/2}(v_n)} \right|. \end{aligned}$$

Then, for the first term

$$\begin{aligned} \left| \frac{\mu_{n-1/2}^N(w_n\varphi)}{\mu_{n-1/2}^N(w_n)} - \frac{\mu_{n-1/2}^N(w_n\varphi)}{\mu_{n-1/2}(v_n)} \right| &= \left| \frac{\mu_{n-1/2}^N(w_n\varphi)}{\mu_{n-1/2}^N(w_n)} \right| \left| \frac{\mu_{n-1/2}(v_n) - \mu_{n-1/2}^N(w_n)}{\mu_{n-1/2}(v_n)} \right| \\ &\leq \frac{\|\varphi\|_\infty}{|\mu_{n-1/2}(v_n)|} |\mu_{n-1/2}(v_n) - \mu_{n-1/2}^N(w_n)|. \end{aligned}$$

For the second term

$$\left| \frac{\mu_{n-1/2}^N(w_n\varphi)}{\mu_{n-1/2}(v_n)} - \frac{\mu_{n-1/2}(v_n\varphi)}{\mu_{n-1/2}(v_n)} \right| = \frac{1}{|\mu_{n-1/2}(v_n)|} |\mu_{n-1/2}^N(w_n\varphi) - \mu_{n-1/2}(v_n\varphi)|.$$

It follows that

$$\begin{aligned} \mathbb{E} [|\mu_n^N(\varphi) - \mu_n(\varphi)|^p]^{1/p} &\leq \frac{\|\varphi\|_\infty}{\mu_{n-1/2}(v_n)} \mathbb{E} [|\mu_{n-1/2}(v_n) - \mu_{n-1/2}^N(w_n)|^p]^{1/p} \\ &\quad + \frac{1}{\mu_{n-1/2}(v_n)} \mathbb{E} [|\mu_{n-1/2}^N(w_n\varphi) - \mu_{n-1/2}(v_n\varphi)|^p]^{1/p} \\ &\leq 2 \frac{\|\varphi\|_\infty}{\mu_{n-1/2}(v_n)} \frac{\tilde{C}_{p,n}(\gamma)}{N^{1/2}}, \end{aligned}$$

where $\mu_{n-1/2}(v_n) = \int \mu_{n-1/2}(x) e^{-\gamma} \pi(x)^{1-e^{-\gamma}} dx$ is the normalising constant of μ_n .

We now show (C.5). Let \mathcal{F}_{n-1}^N denote the σ -field generated by the weighted samples up to (and including) time $n-1$. Consider the decomposition

$$\begin{aligned} \mu_{n-1/2}^N(w_n\varphi) - \mu_{n-1/2}(v_n\varphi) &= \mu_{n-1/2}^N(w_n\varphi) - \mathbb{E} [\mu_{n-1/2}^N(w_n\varphi) | \mathcal{F}_{n-1}^N] \\ &\quad + \mathbb{E} [\mu_{n-1/2}^N(w_n\varphi) | \mathcal{F}_{n-1}^N] - \mu_{n-1/2}(v_n\varphi). \end{aligned}$$

Let us first bound

$$\mathbb{E} [|\mu_{n-1/2}^N(w_n\varphi) - \mathbb{E} [\mu_{n-1/2}^N(w_n\varphi) | \mathcal{F}_{n-1}^N]|^p]^{1/p}.$$

Using the sequence of functions $\Delta_n^i : \mathbb{R}^d \mapsto \mathbb{R}$, $\Delta_n^i(x) := w_n(x)\varphi(x) - \mathbb{E} [w_n(X_n^i)\varphi(X_n^i) | \mathcal{F}_{n-1}^N]$, for $i = 1, \dots, N$. Conditionally on \mathcal{F}_{n-1}^N , $\Delta_n^i(X_n^i)$ $i = 1, \dots, N$ are independent and have expectation equal to 0, moreover

$$\mu_{n-1/2}^N(w_n\varphi) - \mathbb{E} [\mu_{n-1/2}^N(w_n\varphi) | \mathcal{F}_{n-1}^N] = \frac{1}{N} \sum_{i=1}^N \Delta_n^i(X_n^i).$$

Using Lemma C.3, we have almost surely

$$\sqrt{N} \mathbb{E} [|\mu_{n-1/2}^N(w_n\varphi) - \mathbb{E} [\mu_{n-1/2}^N(w_n\varphi) | \mathcal{F}_{n-1}^N]|^p | \mathcal{F}_{n-1}^N]^{1/p} \leq 4b(p)^{1/p} \|w_n\|_\infty \|\varphi\|_\infty, \quad (\text{C.6})$$

where $b(p)$ is given in (C.4).

Consider now the second term and use Proposition C.1

$$\mathbb{E} \left[\mu_{n-1/2}^N(w_n \varphi) | \mathcal{F}_{n-1}^N \right] - \mu_{n-1/2}(v_n \varphi) = \int \varphi(x_n) \pi(x_n)^{1-e^{-\gamma}} \left[\left(\mu_{n-1/2}^N(x_n) \right)^{e^{-\gamma}} - \left(\mu_{n-1/2}(x_n) \right)^{e^{-\gamma}} \right] dx_n.$$

Using Proposition C.2 we find

$$\mathbb{E} \left[\left| \mathbb{E} \left[\mu_{n-1/2}^N(w_n \varphi) | \mathcal{F}_{n-1}^N \right] - \mu_{n-1/2}(v_n \varphi) \right|^p \right]^{1/p} \leq D_{p,n}(\gamma) \frac{\|\varphi\|_\infty}{N^{1/2}} \int \pi(x_n)^{1-e^{-\gamma}} dx_n.$$

It follows that

$$\mathbb{E} \left[\left| \mu_{n-1/2}^N(w_n \varphi) - \mu_{n-1/2}(v_n \varphi) \right|^p \right]^{1/p} \leq \tilde{C}_{p,n} \frac{\|\varphi\|_\infty}{N^{1/2}}$$

holds with $\tilde{C}_{p,n}(\gamma) = 4b(p)^{1/p} \|w_n\|_\infty \|\varphi\|_\infty + D_{p,n}(\gamma)$. \square

We control the error induced by the resampling step using the same argument as Crisan and Doucet [2002, Lemma 5] whose proof is given for completeness.

Lemma C.5 (Multinomial resampling). *Under the conditions of Proposition 3.2, assume that for any $\varphi \in \mathcal{B}_b(\mathbb{R}^d)$, for some $p \geq 1$ and some finite constant $\bar{C}_{p,n}$*

$$\mathbb{E} \left[\left| \mu_n^N(\varphi) - \mu_n(\varphi) \right|^p \right]^{1/p} \leq \bar{C}_{p,n} \frac{\|\varphi\|_\infty}{N^{1/2}},$$

then after the resampling step performed through multinomial resampling

$$\mathbb{E} \left[\left| \tilde{\mu}_n^N(\varphi) - \mu_n(\varphi) \right|^p \right]^{1/p} \leq C_{p,n}(\gamma) \frac{\|\varphi\|_\infty}{N^{1/2}}$$

for any $\varphi \in \mathcal{B}_b(\mathbb{R}^d)$ and $C_{p,n}(\gamma) = 4b(p)^{1/p} + \bar{C}_{p,n}(\gamma)$.

Proof. Divide into two terms and apply Minkowski's inequality

$$\begin{aligned} \mathbb{E} \left[\left| \tilde{\mu}_n^N(\varphi) - \mu_n(\varphi) \right|^p \right]^{1/p} &\leq \mathbb{E} \left[\left| \tilde{\mu}_n^N(\varphi) - \mu_n^N(\varphi) \right|^p \right]^{1/p} \\ &\quad + \mathbb{E} \left[\left| \mu_n^N(\varphi) - \mu_n(\varphi) \right|^p \right]^{1/p}. \end{aligned}$$

Denote by \mathcal{F}_n^N the σ -field generated by the weighted samples up to (and including) time n , $\mathcal{F}_n^N := \sigma(X_n^i : i \in \{1, \dots, N\}) \vee \mathcal{G}_{n-1}^N$ and consider the sequence of functions $\Delta_n^i : E \mapsto \mathbb{R}$, $\Delta_n^i(x) := \varphi(x) - \mathbb{E} \left[\varphi(\tilde{X}_n^i) | \mathcal{F}_n^N \right]$, for $i = 1, \dots, N$. Conditionally on \mathcal{F}_n^N , $\Delta_n^i(\tilde{X}_n^i)$ $i = 1, \dots, N$ are independent and have expectation equal to 0, moreover

$$\tilde{\mu}_n^N(\varphi) - \mu_n^N(\varphi) = \frac{1}{N} \sum_{i=1}^N \left(\varphi(\tilde{X}_n^i) - \mathbb{E} \left[\varphi(\tilde{X}_n^i) | \mathcal{F}_n^N \right] \right) = \frac{1}{N} \sum_{i=1}^N \Delta_n^i(\tilde{X}_n^i).$$

Using Lemma C.3, we find

$$\sqrt{N} \mathbb{E} \left[\left| \tilde{\mu}_n^N(\varphi) - \mu_n^N(\varphi) \right|^p | \mathcal{F}_n^N \right]^{1/p} \leq 4b(p)^{1/p} \|\varphi\|_\infty, \quad (\text{C.7})$$

where $b(p)$ is as in (C.4). This result combined with the hypothesis yields

$$\mathbb{E} \left[\left| \tilde{\mu}_n^N(\varphi) - \mu_n(\varphi) \right|^p \right]^{1/p} \leq 4b(p)^{1/p} \frac{\|\varphi\|_\infty}{N^{1/2}} + \bar{C}_{p,n}(\gamma) \frac{\|\varphi\|_\infty}{N^{1/2}} \leq (4b(p)^{1/p} + \bar{C}_{p,n}(\gamma)) \frac{\|\varphi\|_\infty}{N^{1/2}}.$$

Thus, $C_{p,n}(\gamma) = 4b(p)^{1/p} + \bar{C}_{p,n}(\gamma)$. \square

D Analytic solutions: Multivariate Gaussian case

This section focuses on comparing the evolution of the PDEs introduced in this section for the special case of transporting a Gaussian $\mu_0(x) = \mathcal{N}(x; m_0, C_0)$ to target Gaussian $\pi(x) = \mathcal{N}(x; m_\pi, C_\pi)$. In this case, we can obtain nice expressions for the moments along the flow described by each PDE.

In particular, observing that both the tempered W flow and the tempered FR flow preserve gaussianity, we have that $\mu_t(x) = \mathcal{N}(x; m_t, C_t)$ for each time $t \geq 0$.

We detail here the results needed to obtain the ODEs describing the tempered and standard PDEs for the special case of transporting a Gaussian $\mu_0(x) = \mathcal{N}(x; m_0, C_0)$ to target Gaussian $\pi(x) = \mathcal{N}(x; m_\pi, C_\pi)$.

Wasserstein Flow (Langevin) The PDE in this case is the Fokker-Planck equation for the overdamped Langevin SDE

$$\begin{aligned} dX_t &= -\nabla V_\pi(X_t)dt + \sqrt{2}dB_t \\ &= -C_\pi^{-1}(X_t - m_\pi)dt + \sqrt{2}dB_t. \end{aligned}$$

Since the potential takes the form $V_\pi(x) = \frac{1}{2}(x - m_\pi)^\top C_\pi^{-1}(x - m_\pi)$, the moment equations are standard as this essentially boils down to an Ornstein-Uhlenbeck process. They are given by

$$\begin{aligned} \dot{m}_t &= -C_\pi^{-1}(m_t - m_\pi) \\ \dot{C}_t &= -C_\pi^{-1}C_t - C_t C_\pi^{-1} + 2I \end{aligned}$$

and the explicit solution can be found as

$$\begin{aligned} m_t &= e^{-tC_\pi^{-1}} m_0 + (I - e^{-tC_\pi^{-1}})m_\pi \\ C_t &= e^{-tC_\pi^{-1}} \left(2 \int_0^t e^{sC_\pi^{-1}} (e^{sC_\pi^{-1}})^\top ds + C_0 \right) (e^{-tC_\pi^{-1}})^\top. \end{aligned}$$

In the 1D case, we can easily evaluate the expression for C_t as

$$C_t = e^{-2tC_\pi^{-1}} [C_0 + C_\pi(e^{2tC_\pi^{-1}} - 1)].$$

Fisher–Rao flow In the Gaussian case, the ODEs for the mean and covariance respectively are given by

$$\begin{aligned} \dot{m}_t &= -C_t C_\pi^{-1}(m_t - m_\pi) \\ \dot{C}_t &= -C_t C_\pi^{-1}C_t + C_t. \end{aligned}$$

The explicit solutions in this case are known (see e.g. Chen et al. [2023, Lemma E.3]),

$$\begin{aligned} m_t &= m_\pi + e^{-t} \left((1 - e^{-t})C_\pi^{-1} + e^{-t}C_0^{-1} \right)^{-1} C_0^{-1}(m_0 - m_\pi) \\ &= m_\pi + e^{-t} C_t C_0^{-1}(m_0 - m_\pi) \\ C_t^{-1} &= C_\pi^{-1} + e^{-t}(C_0^{-1} - C_\pi^{-1}). \end{aligned}$$

Wasserstein–Fisher–Rao flow The mean and covariance equations in the Gaussian case for the Wasserstein–Fisher–Rao flow can be obtained using the results for the pure Wasserstein and pure Fisher–Rao flows as shown in Liero et al. [2025, Proposition 2.2],

$$\begin{aligned} \dot{m}_t &= -(C_t + I)C_\pi^{-1}(m_t - m_\pi) \\ \dot{C}_t &= -C_t C_\pi^{-1}C_t + C_t - C_\pi^{-1}C_t - C_t C_\pi^{-1} + 2I \end{aligned}$$

The explicit solution in the 1D case is given by

$$\begin{aligned} C_t &= C_\pi + \frac{1}{\left(\frac{1}{C_0 - C_\pi} + \frac{1}{C_\pi + 2} \right) e^{(1 + \frac{2}{C_\pi})t} - \frac{1}{C_\pi + 2}} \\ m_t &= m_\pi + (m_0 - m_\pi) \exp\left(\frac{t}{C_\pi} \right) \frac{C_t - C_\pi}{C_0 - C_\pi}, \end{aligned}$$

showing that C_t must approach C_π faster than $\exp(t/C_\pi)$ grows, which is guaranteed by the factor 2 in the expression for C_t . Explicit solution of the covariance evolution under the WFR flow are given in Liero et al. [2025, Remark 2.3].

E Birth Death Langevin Algorithms

Birth Death Langevin (BDL) algorithms were introduced in [Lu et al., 2023, 2019] as an approximation of the WFR flow. They consider the PDE (2.3) and replace μ_t with an empirical measure leading to an interacting particle system whose evolution is then discretised in time. The W step is performed via the unadjusted Langevin algorithm (ULA) with target π , as in (3.4); while the FR step is performed via a birth-death step with exact rate

$$\Lambda(x, \mu_t) := \log\left(\frac{\mu_t}{\pi}\right) - \mathbb{E}_{\mu_t}\left[\log\left(\frac{\mu_t}{\pi}\right)\right]. \quad (\text{E.1})$$

When μ_t is replaced by an empirical measure μ_t^N , the rate $\Lambda(x, \mu_t)$ cannot be computed analytically and [Lu et al., 2019] resort to kernel density estimation (KDE) and replace μ_t^N with $K_\varepsilon * \mu_t^N$, where K_ε is a kernel with bandwidth ε . Convergence of the resulting continuous-time interacting particle system is guaranteed by Lu et al. [2019, Proposition 5.1].

Contrary to our approach, the BDL dynamics are obtained by first applying a space discretisation (corresponding to the empirical measure μ_t^N) and then a time discretisation. The W step described by the Fokker–Planck PDE (2.1) is resolved using a time discretisation of the corresponding Langevin SDE and the FR flow (2.2) is resolved through its connections with birth-death processes. Different approximations of the rate (E.1) lead to slightly different BDL algorithms [Lu et al., 2023, Pampel et al., 2023].

Algorithm 3 Birth-death accelerate Langevin algorithm (BDL; [Lu et al., 2019])

Inputs: Discretisation steps $(\gamma_n)_{n=1, \dots, T}$, kernel function K , initial proposal μ_0 .

Initialize: sample $X_0^i \sim \mu_0$ for $i = 1, \dots, N$.

for $n = 1, \dots, T$ **do**

Langevin step: $X_n^i = X_{n-1}^i + \gamma_n \nabla \log \pi(X_{n-1}^i) + \sqrt{2\gamma_n} \xi_i$ where $\xi_i \sim \mathcal{N}(0, 1)$ for $i = 1, \dots, N$.

Birth-death step: compute the rate

$$\beta_i = \log\left(N^{-1} \sum_{j=1}^N K(X_n^i - X_n^j)\right) - \log \pi(X_n^i)$$

for $i = 1, \dots, N$.

Birth-death step: set $\bar{\beta}_i = \beta_i - N^{-1} \sum_{j=1}^N \beta_j$. If $\bar{\beta}_i > 0$ kill X_n^i with probability $1 - \exp(-\bar{\beta}_i \gamma_n)$, otherwise duplicate X_n^i w.p. $1 - \exp(\bar{\beta}_i \gamma_n)$.

Resampling: Let N_1 denote the current number of particles.

if $N_1 > N$ **then**

Kill $N_1 - N$ randomly selected particles.

else

Duplicate $N - N_1$ randomly selected particles.

end if

end for

Output: $\{X_n^i\}_{i=1}^N$.

The birth-death Langevin algorithm of [Lu et al., 2019] is given in Algorithm 3. [Lu et al., 2023] replace the average rate in Algorithm 3 is replaced by $\bar{\beta}_i = \beta_i - N^{-1} \sum_{j=1}^N \beta_j + \sum_{j=1}^N \frac{K(X_n^i - X_n^j)}{\sum_{l=1}^N K(X_n^j - X_n^l)} - 1$.

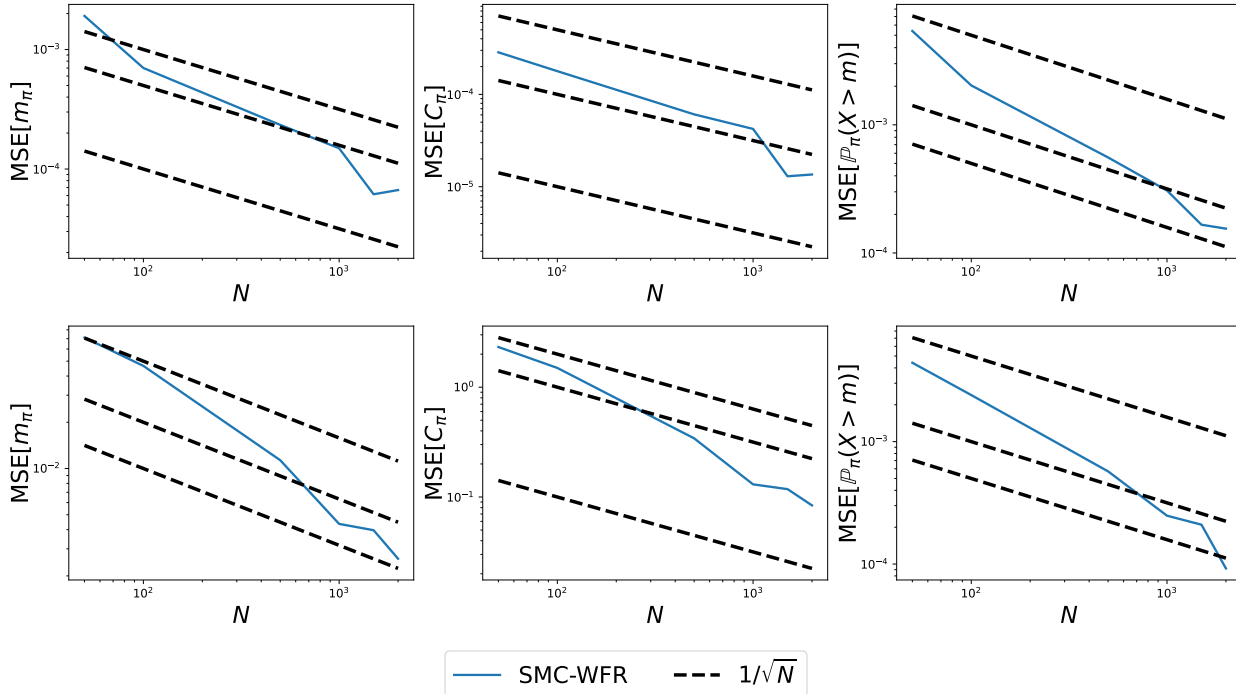


Figure F.1: Decay of MSE for mean, variance and $\mathbb{P}_\pi(X > m_\pi)$ of $\pi(x) = \mathcal{N}(x; 20, 0.1)$ (first row), $\pi(x) = \mathcal{N}(x; 1, 5)$ for increasing number of particles N (in blue); we add the theoretical rate C/\sqrt{N} for a given constant C for reference (in dashed black). The results are averaged over 50 replicates.

F Additional Experimental Results

F.1 Confirmation of rate in Proposition 3.2

We empirically validate our convergence result in Proposition 3.2 using a simple Gaussian example with initial distribution $\mu_0(x) = \mathcal{N}(x; 0, 1)$ and targets $\pi(x) = \mathcal{N}(x; 20, 0.1)$ and $\pi(x) = \mathcal{N}(x; 1, 5)$. In the first case the WFR flow is mostly driven by the W part while for the second target the FR part drives the KL decay.

We set $\gamma = 10^{-2}$ and iterate for 400 steps. We consider number of particles $N = 50, 100, 500, 1000, 1500, 2000$. Figure F.1 shows the square root of the mean squared error (MSE) for mean and variance of π and $\mathbb{P}_\pi(X > m_\pi)$. We add the theoretical rate in Proposition 3.2 for reference. As is often the case, for small N the decay is faster than \sqrt{N} , but as $N \rightarrow \infty$ the MSE decays at the predicted rate.

F.2 SMC-ULA and SMC-MALA as Approximations of the WFR Flow

Figure F.2 shows the evolution of KL given by Algorithm 1 and the SMC-ULA and SMC-MALA algorithms described in Section 4.4 for three 1D targets

$$\begin{aligned} \pi(x) &= \mathcal{N}(x; 20, 0.1) \\ \pi(x) &= \mathcal{N}(x; 1, 5) \\ \pi(x) &= \frac{1}{2}\mathcal{N}(x; 0, 1) + \frac{1}{2}\mathcal{N}(x; 6, 1). \end{aligned}$$

The initial distribution is a standard Gaussian. The plots suggest that SMC-ULA and SMC-MALA are poor approximations of the WFR flow. In particular, for the first target, convergence is driven by the W flow (approximated by ULA or MALA) and thus the three algorithms are all in agreement with the exact flow. For the second target, convergence is driven by the FR flow. Figure F.2 middle shows that the

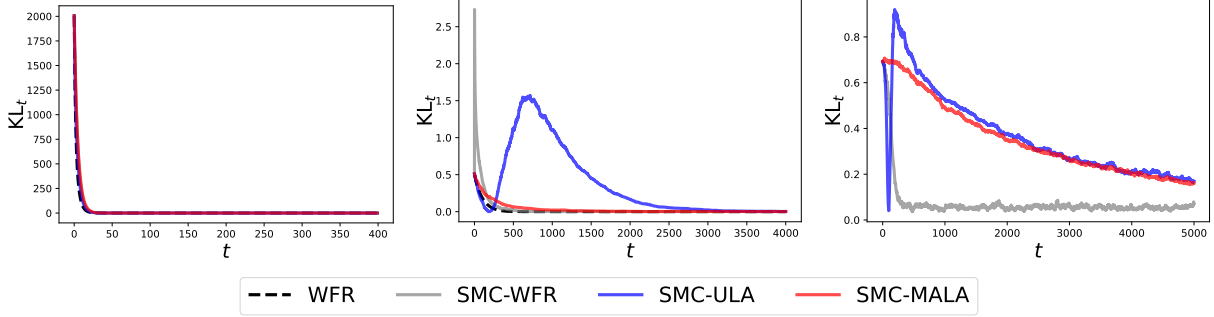


Figure F.2: SMC-ULA and SMC-MALA as approximations of WFR: Comparison of evolution of KL of the exact WFR flow and approximations provided by Algorithm 1, SMC-ULA, SMC-MALA with initial distribution $\mu_0(x) = \mathcal{N}(x; 0, 1)$ and $\pi(x) = \mathcal{N}(x; 20, 0.1)$ (left), $\pi(x) = \mathcal{N}(x; 1, 5)$ (middle), $\pi(x) = \frac{1}{2}\mathcal{N}(x; 0, 1) + \frac{1}{2}\mathcal{N}(x; 6, 1)$ (right).

cheaper alternative to the weights (4.5) used in SMC-ULA performs poorly in this case. The third target is non-Gaussian, in this case both SMC-ULA and SMC-MALA exhibit slower convergence than SMC-WFR.

F.3 Comparison with other Monte Carlo algorithms

We collect here additional experimental details for Section 5.3. The targets we consider are summarised in Table 2.

Target	d	$\pi(x)$	Behaviour
Gaussian mixture	2	$\sum_{i=1}^4 w_i \mathcal{N}(x; \mathbf{m}_i, \Sigma_i)$	multimodality
Banana	2	$\exp(-[\sigma^2(x_2 - x_1^2)^2/2 + (1-x_1)^2/2\sigma^2])$	multiscale/ locally Lipschitz gradient
Donut	2	$\exp(-(\sqrt{x_1^2 + x_2^2} - 2)^2/0.25^2)$	concentration
Gaussian	20	$\mathcal{N}(x; \mathbf{m}, \Sigma)$	high dimensional
Gaussian mixture	20	$\sum_{i=1}^c w_i \mathcal{N}(x; \mathbf{m}_i, \Sigma_i)$	multimodality/ high dimensional

Table 2: Summary of target distributions (up to normalisation) and their challenges.

2D Gaussian mixture (Figure 5.3) The 2D 4 component Gaussian mixture is given by $\pi(x) = \sum_{i=1}^4 w_i \mathcal{N}(x; \mathbf{m}_i, \Sigma_i)$ with

$$w = \left[\frac{1}{3}, \frac{1}{6}, \frac{1}{3}, \frac{1}{6} \right]^\top; \quad \mathbf{m}_1 = [3, 3]^\top; \quad \mathbf{m}_2 = [9, 10]^\top; \quad \mathbf{m}_3 = [2, 2]^\top; \quad \mathbf{m}_4 = [10, 4]^\top$$

$$\Sigma_1 = 0.7 \cdot \begin{bmatrix} 1 & -0.8377 \\ -0.8377 & 1 \end{bmatrix}; \quad \Sigma_2 = 0.7 \cdot \begin{bmatrix} 1 & 0.8377 \\ 0.8377 & 1 \end{bmatrix}; \quad \Sigma_3 = \Sigma_1; \quad \Sigma_4 = 2 \cdot \begin{bmatrix} 1 & -0.6701 \\ -0.6701 & 1 \end{bmatrix}.$$

For the 2D Gaussian mixture target we use $N = 300, \gamma = 0.2$. We tune the variance of the proposal for MALA and SMC-MALA to achieve 57% acceptance rate and the variance of RWM for SMC tempering to achieve 23% acceptance rate.

We use $T = 1000$ iterations for SMC-WFR. The number of iterations of the other algorithms is selected so that the runtime of all algorithms is comparable.

For the 2D Gaussian Mixture ULA does not work well and fails to explore all modes. A similar issue affects MALA and SMC-MALA. SMC-ULA gives the worst results as it combines the lack of exploration of

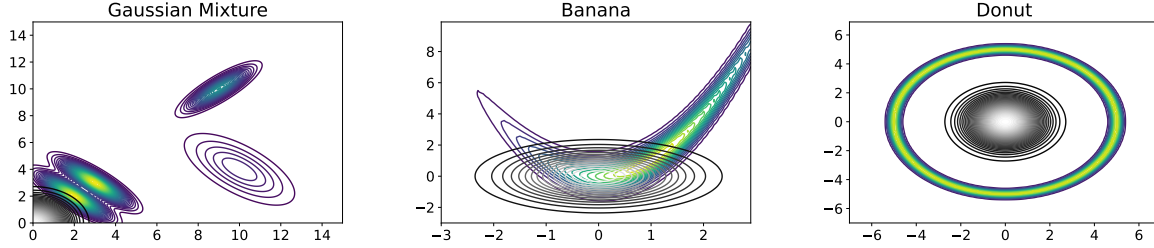


Figure F.3: Contour plots for 2D targets (Gaussian Mixture, Banana and Donut) and initial distribution $\mu_0(x) = \mathcal{N}(x; 0, 1)$.

ULA with the instability in the weights (4.8) due to the lack of overlap between μ_0 and π (see Figure F.3).

SMC-tempering works well in this setting, as the tempering iterates (4.6) flatten the target in the early iterations and help with global exploration. SMC-WFR combines the local exploration of ULA with the ability to jump from one mode to another and has the fastest convergence, although it has a larger bias than SMC-tempering due to the large value of γ selected. On the other hand, the fast convergence of SMC-WFR occurs only for sufficiently large γ .

Banana (Figure F.4) For the banana target we select $\sigma^2 = 2$. We use $N = 300, \gamma = 0.005$. We tune the variance of the proposal for MALA and SMC-MALA to achieve 57% acceptance rate and the variance of RWM for SMC tempering to achieve 23% acceptance rate. We use $T = 4000$ iterations for SMC-WFR. The number of iterations of the other algorithms is selected so that the runtime of all algorithms is comparable.

For the banana target ULA and SMC-ULA are slower to convergence as in the initial stages the drift component of ULA pushes the particles far in the tails. SMC-WFR does not suffer from this instability despite the ULA proposal. This experiment showcases the benefit of using the weights (3.5) rather than (4.8) despite the additional computational cost.

MALA and SMC-MALA provide the best results. SMC-tempering has similar convergence speed but tends to underestimate the covariance matrix.

Donut (Figure F.5) For the donut target we use $N = 300, \gamma = 0.005$. We tune the variance of the proposal for MALA and SMC-MALA to achieve 57% acceptance rate and the variance of RWM for SMC tempering to achieve 23% acceptance rate. We use $T = 1000$ iterations for SMC-WFR. The number of iterations of the other algorithms is selected so that the runtime of all algorithms is comparable.

For the donut target ULA works well while SMC-tempering struggles to quickly move from μ_0 to π since it does not use gradient information. SMC-WFR and SMC-ULA improve the results of ULA as guaranteed by the converge results of WFR (2.5). For this target SMC-ULA and SMC-WFR behave similarly, we do not observe any numerical instability in SMC-ULA as μ_0 significantly overlaps with π (see Figure F.3) and the weights (4.8) are stable.

SMC-tempering is slow to convergence due to the lack of gradient information.

20D Gaussian (Figure F.6 and F.7) We consider two 20D Gaussian distributions (thus ∇V_π is globally Lipschitz continuous). One in which the W flow performs well since the log-Sobolev constant is small (and so C_{LSI}^{-1} is large) and a second one in which the log-Sobolev constant is large and thus the W flow performs less well. The first target has

$$\begin{aligned} \mathbf{m} &= 3 \cdot \mathbf{1}_{20} \\ \Sigma &= 2 \cdot C \end{aligned}$$

where $\mathbf{1}_{20}$ is the 20D one vector. The correlation matrix C can be found in the supplementary material, in this case $C_{\text{LSI}} = 0.077$. The second target has

$$\begin{aligned} \mathbf{m} &= 20 \cdot \mathbf{1}_{20} \\ \Sigma &= 5 \cdot \text{Id}_{20 \times 20} \end{aligned}$$

where $\text{Id}_{20 \times 20}$ is the 20D identity matrix. In this case $C_{\text{LSI}} = 5$.

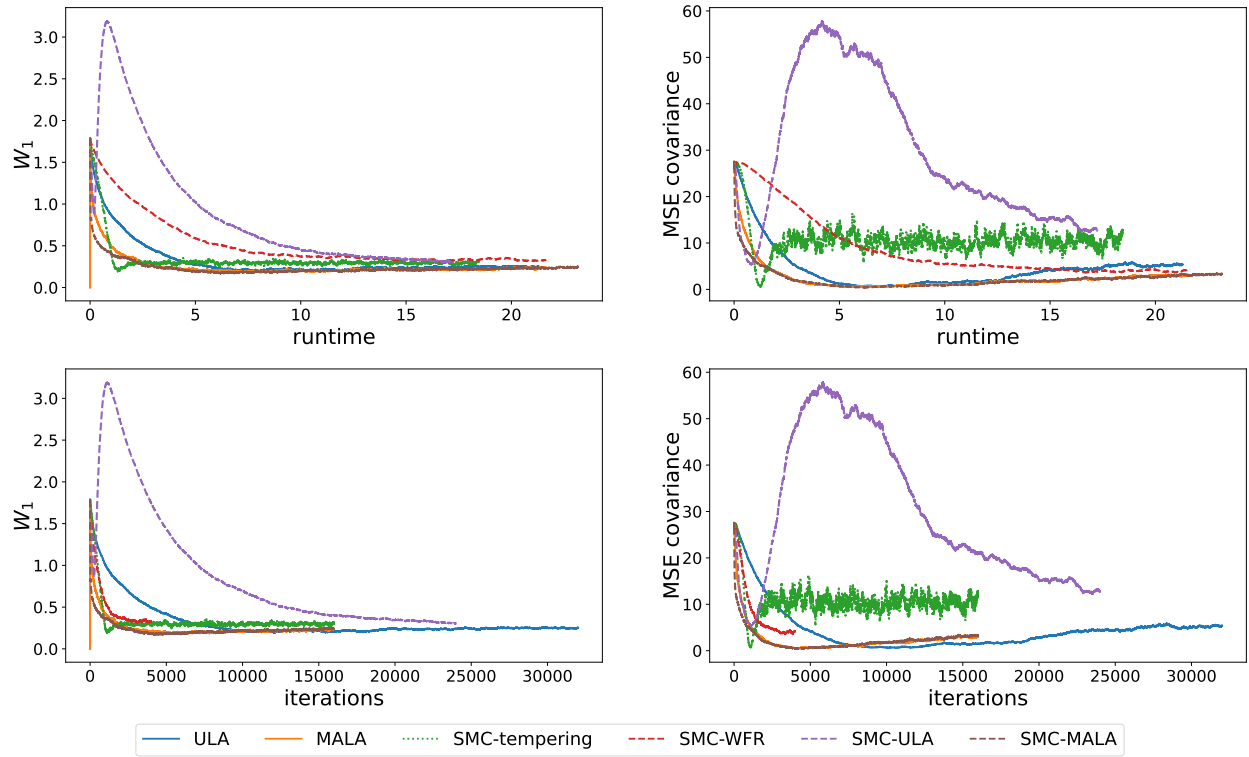


Figure F.4: Banana: Evolution of W_1 and mean squared error (MSE) for the covariance matrix against runtime (first row) and number of iterations (second row) averaged over 50 repetitions. The initial distribution is $\mu_0(x) = \mathcal{N}(x; 0, \text{Id})$. We compare ULA, MALA, SMC tempering, SMC-WFR, SMC-ULA and SMC-MALA.

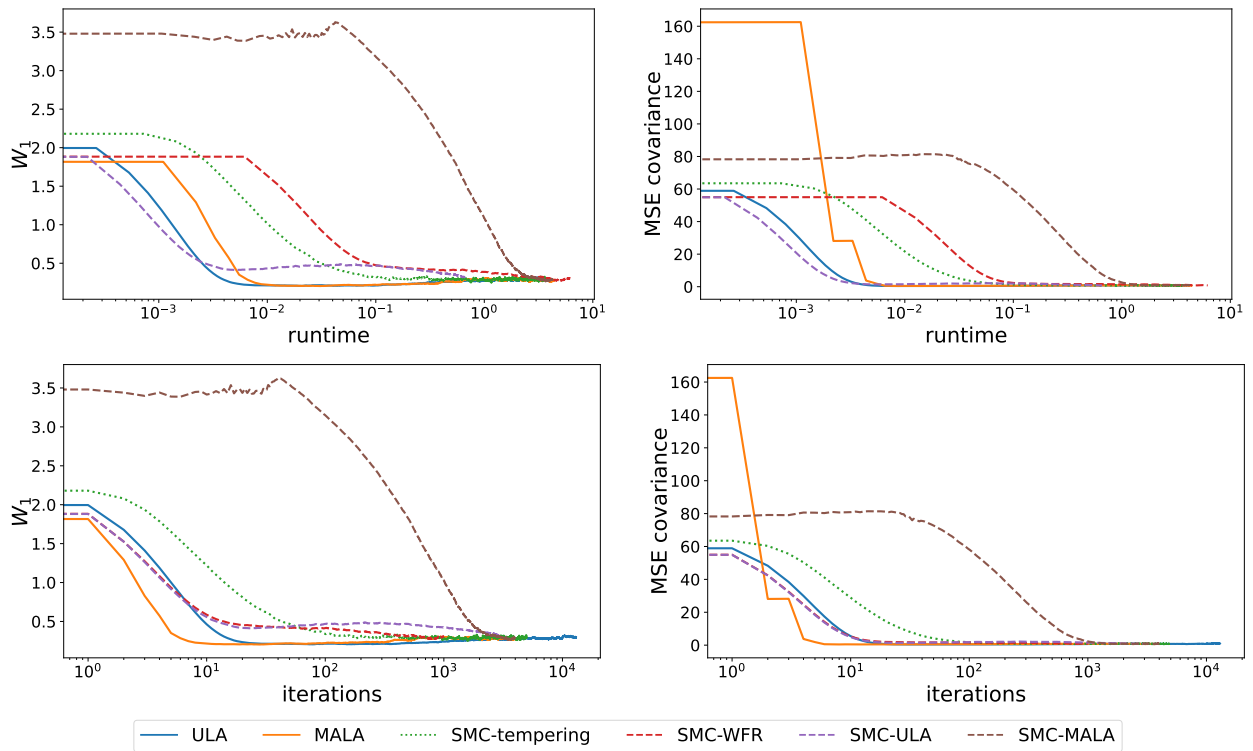


Figure F.5: Donut (ULA works well): Evolution of W_1 and mean squared error (MSE) for the covariance matrix against runtime (first row) and number of iterations (second row) averaged over 50 repetitions. The initial distribution is $\mu_0(x) = \mathcal{N}(x; 0, \text{Id})$. We compare ULA, MALA, SMC tempering, SMC-WFR, SMC-ULA and SMC-MALA. ULA, SMC-ULA, SMC-WFR are similar in terms of number of iterations but ULA is faster in terms of wallclock time.

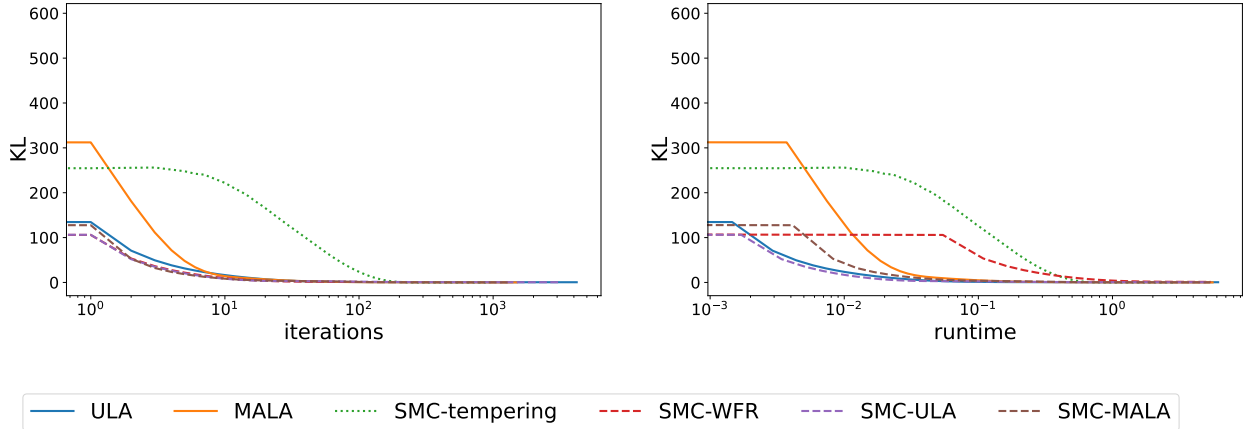


Figure F.6: 20D Gaussian with small log-Sobolev constant (ULA works well): Evolution of KL against runtime (right) and number of iterations (left) averaged over 50 repetitions. The initial distribution is $\mu_0(x) = \mathcal{N}(x; 0, \text{Id})$. We compare ULA, MALA, SMC tempering, SMC-WFR, SMC-ULA and SMC-MALA. SMC-WFR and SMC-ULA achieve the fastest convergence in number of iterations but SMC-ULA and ULA are faster than SMC-WFR in terms of runtime due to their lower computational cost.

For both targets we use $N = 1000$ particles and $T = 100$ iterations for SMC-WFR. The number of iterations of the other algorithms is selected so that the runtime of all algorithms is comparable. We set $\gamma = 0.05$ for target 1 and $\gamma = 0.5$ for target 2. We tune the variance of the proposal for MALA and SMC-MALA to achieve 57% acceptance rate and the variance of RWM for SMC tempering to achieve 23% acceptance rate.

For the first 20D Gaussian target (small log-Sobolev constant) the theory suggests that the W flow is faster than FR. This is confirmed by Figure F.6 which shows SMC-WFR, SMC-ULA and SMC-MALA outperforming both ULA and SMC-tempering on this target in terms of iterations. However, ULA works well and is cheap compared to alternatives and is the faster than SMC-WFR to convergence when taking runtime into account. In this case, SMC-ULA seems to offer the best of both worlds by closely following the WFR flow (approximated by SMC-WFR) and being computationally cheap.

For the second 20D Gaussian target (large log-Sobolev constant) ULA is less fast and in fact MALA based algorithms tend to perform better compared to ULA based ones. SMC-ULA and SMC-WFR perform similarly in terms of iteration number suggesting that in this case SMC-ULA is a valid alternative to approximate the WFR flow.

20D Gaussian mixture (Figure 5.4) The 20D 3 component Gaussian mixture is given by $\pi(x) = \sum_{i=1}^3 w_i \mathcal{N}(x; \mathbf{m}_i, \Sigma_i)$ with

$$w = \left[\frac{1}{2}, \frac{1}{3}, \frac{1}{6} \right]^\top; \quad \mathbf{m}_1 = 3 \cdot \mathbf{1}_{20}; \quad \mathbf{m}_2 = 4 \cdot \mathbf{1}_{20}; \quad \mathbf{m}_3 = [2, 5, \dots, 2, 5]^\top$$

$$\Sigma_1 = 2 \cdot C; \quad \Sigma_2 = 2 \cdot C; \quad \Sigma_3 = C^{-1} M^{-1}$$

where $\mathbf{1}_{20}$ is the 20D one vector. The correlation matrices C, M can be found in the supplementary material.

For the 20D Gaussian mixture target we use $N = 1000, \gamma = 0.1$. We tune the variance of the proposal for MALA and SMC-MALA to achieve 57% acceptance rate and the variance of RWM for SMC tempering to achieve 23% acceptance rate.

We use $T = 1000$ iterations for SMC-WFR. The number of iterations of the other algorithms is selected so that the runtime of all algorithms is comparable.

For the 20D Gaussian Mixture ULA, MALA, SMC-ULA and SMC-MALA do not work well due to the different covariance structure of the 3 components. SMC-tempering also fails on this target. SMC-WFR is the only algorithm to correctly recover the covariance structure of the target.

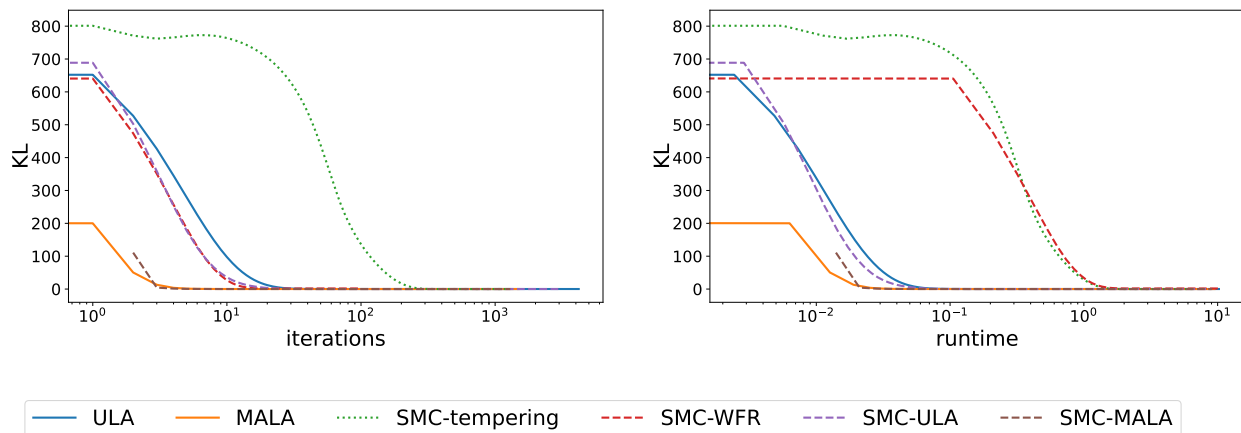


Figure F.7: 20D Gaussian with large log-Sobolev constant (ULA struggles): Evolution of KL against runtime (right) and number of iterations (left) averaged over 50 repetitions. The initial distribution is $\mu_0(x) = \mathcal{N}(x; 0, \text{Id})$. We compare ULA, MALA, SMC tempering, SMC-WFR, SMC-ULA and SMC-MALA. SMC-WFR and SMC-ULA are better than ULA in terms of iteration number. MALA and SMC-MALA outperform ULA based algorithms thanks to tuning of proposal variance.